Atmospheric Research 316 (2025) 107947

Contents lists available at ScienceDirect

Atmospheric Research

journal homepage: www.elsevier.com/locate/atmosres

A multiscale analysis of the Dolores, Uruguay, tornadoes of 6 December 2012 and 15 April 2016

Maurício I. Oliveira [a,b,*], Murilo M. Lopes [b], Vitor Goede [c,d], Marcelo Barreiro [e], Paola M. Salio [f,g,h], Eliton L. Figueiredo [i], Ming Xue [j]

[a] Instituto Nacional de Pesquisas da Amazônia (INPA), Manaus, Amazonas, Brazil
[b] Grupo de Modelagem Atmosférica, Departamento de Física, Univerisade Federal de Santa Maria, Santa Maria, Rio Grande do Sul, Brazil
[c] School of Meteorology, University of Oklahoma, Norman, OK, United States
[d] Advanced Radar Research Center (ARRC), and School of Meteorology, University of Oklahoma, Norman, OK, United States
[e] Departamento de Ciencias de la Atmósfera y Física de los Océanos, Facultad de Ciencias, Universidad de la República, Montevideo 11400, Uruguay
[f] Instituto Franco-Argentino de Estudios sobre el Clima y sus Impactos (IFAECI) – IRL 3351 – CNRS-CONICET-IRD-UBA, Buenos Aires, Argentina
[g] CONICET – Universidad de Buenos Aires, Centro de Investigaciones del Mar y la Atmósfera (CIMA), Buenos Aires, Argentina
[h] Universidad de Buenos Aires, Facultad de Ciencias Exactas y Naturales, Departamento de Ciencias de la Atmósfera y los Océanos (DCAO), Buenos Aires, Argentina
[i] Centro de Pesquisas e Previsões Meteorológicas, Universidade Federal de Pelotas, Pelotas, Rio Grande do Sul, Brazil
[j] Center for Analysis and Prediction of Storms, and School of Meteorology, University of Oklahoma, Norman, OK, United States

ARTICLE INFO

Keywords:
Dolores tornadoes
Severe convection
Tornado tracks
Mesoscale environments
Supercells
Southeastern South America

ABSTRACT

On 15 April 2016, a destructive tornado impacted the town of Dolores, in the Department of Soriano, southwestern Uruguay (SWUY), resulting in one of the most damaging, single-event weather disasters in Uruguay's history. Remarkably, another strong tornado hit Dolores less than four years earlier on 6 December 2012, causing damage in the south portion of the town. This study investigates the Dolores tornado cases in order to document and compare them, with emphasis on the synoptic- and mesoscale environments that led to the two events. It is shown that both tornadoes occurred far downstream of upper-level troughs, under strong mid- and high-level northwesterly winds, and in warm sectors north of warm fronts in southern Uruguay. Key to the development of the tornadic storms was the presence of northwesterly low-level jets that were instrumental in building up conditional instability and low-level shear for tornadic supercells. Based on the the presence of enhanced lines of cumulus clouds noted on visible satellite imagery, it is speculated that local breeze circulations at the northern edge of the Parana river delta or outflow boundaries may have played a role in fostering storm initiation near the Argentina-Uruguay border, although the available data is insufficient to allow for in-depth analyses of these features. Reanalysis-derived soundings reveal that, upon formation, the storms developed in environments characterized by robust conditional instability, deep-layer shear, low-level helicity, low lifting condensation levels, and weak-to-modest convective inhibition, all ingredients favorable for supercell tornado development. This study stresses the need for more research addressing tornadoes in Uruguay and proposes some avenues for future research.

1. Introduction

The occurrence of tornadic storms in southeastern South America (SESA) (Fig. 1) has been highlighted for many decades (Fujita, 1973; Schwarzkopf, 1988; Dyer, 1988; Silva Dias and Grammelsbacher, 1991; Brooks et al., 2003, 2019; Silva Dias, 2011; Nascimento et al., 2014; Rasmussen et al., 2014; Oliveira et al., 2022a; Ferreira et al., 2022; Veloso-Aguila et al., 2023; dos Santos et al., 2023; Lopes and Nascimento, 2024). Most significant tornadoes in SESA seem to occur in a corridor that stretches from central-eastern Argentina northward into northern Argentina (Schwarzkopf and Rosso, 1982; Schwarzkopf, 1988; Rasmussen et al., 2014; Pita and de Schwarzkopf, 2016; Veloso-Aguila et al., 2023), Paraguay (Dyer, 1988; Veloso-Aguila et al., 2023), Uruguay (Fujita, 1973; Durañona, 2015; Veloso-Aguila et al., 2023; Lopes and Nascimento, 2024), and southern/southeastern/central-western Brazil (Silva Dias and Grammelsbacher, 1991; Agostinho

* Corresponding author.
E-mail address: mauricio.meteorologia@gmail.com (M.I. Oliveira).

https://doi.org/10.1016/j.atmosres.2025.107947
Received 16 July 2024; Received in revised form 16 January 2025; Accepted 20 January 2025
Available online 27 January 2025

et al., 2005; Silva Dias, 2011; Nascimento et al., 2014; Oliveira et al., 2022a; Ferreira et al., 2022; Lopes and Nascimento, 2024). The occurrence of deep convection supporting severe weather in SESA is fostered by a regular juxtaposition of large convective available potential energy (>1000 J kg^{-1}) and deep-layer bulk shear (>20 m s^{-1}) (Rasmussen and Blanchard, 1998; Brooks et al., 2003; Taszarek et al., 2021; Piscitelli et al., 2022; dos Santos et al., 2023; Lopes and Nascimento, 2024) in tandem with low lifting condensation level heights (<1000 m) and boundary layer bulk shear (>10 m s^{-1}) (Veloso-Aguila et al., 2023; Lopes and Nascimento, 2024). In spite of the propensity for tornadic activity in SESA (Veloso-Aguila et al., 2023; Lopes and Nascimento, 2024; Salio et al., 2024), tornado documentation has historically been unsystematic in that region (Fujita, 1973; Schwarzkopf, 1988; Silva Dias and Grammelsbacher, 1991; Nascimento and Doswell III, 2006) and only a very small number of case studies have been conducted to analyze tornado events in depth (Silva Dias and Grammelsbacher, 1991; Nascimento et al., 2014; Oliveira et al., 2022a; Ferreira et al., 2022). In very recent years, however, regional and integrated initiatives have fostered systematic documentation of tornadoes and other severe storm phenomena in SESA (Salio et al., 2024).

Among the countries of SESA, Uruguay is the only one located entirely within the South American "tornado alley" (Lopes and dos Santos, 2022). Nevertheless, formal documentation and in-depth analyses of tornado events in Uruguay have remained scarce in the literature. In this sense, other high-impact, widespread meteorological hazards such as precipitation extremes (e.g., Ungerovich and Barreiro, 2019; Ungerovich et al., 2023) have received more attention. The difficulty of studying tornadoes and their parent convective storms in Uruguay stems from the serendipitousness of tornado reports amid sparsely populated areas,[1] the absence of Doppler radars, and sparse observational networks. In Uruguay, as in other tornado-prone areas worldwide, the insufficient documentation of tornadoes, as well as any other types of small-scale hazardous convective phenomena, often leads to a deceiving and dangerous public perception that these phenomena are unlikely ever to occur. Such a condition may, in turn, lead to an underestimate of the actual threat posed by tornadoes and, consequently, undermine efforts to study and predict this type of phenomenon. As a result, the population and infrastructure in Uruguay, much like most of the countries in South America, are rather vulnerable to tornado hazards (Barrett et al., 2020; Marín et al., 2021; Vicencio et al., 2021).

During the afternoon of 15 April 2016, a destructive tornado struck the town of Dolores (population 20,000), located in the Department of Soriano, southwestern Uruguay (SWUY). The tornado formed just west of Dolores and intensified as it crossed the town, causing 5 fatalities and over 200 injuries (Becker, 2016; Beer, 2023). Significant damage was reported in Dolores, with over 200 houses and businesses partially or totally destroyed; total losses were estimated at US $-35 million (Beer, 2023), making this tornado one of the most damaging weather-related disasters in Uruguay's history. The national weather service (INUMET) produced a technical report describing the overall meteorological conditions that lead to the tornado development, its path, and assigned to it a category F2/F3 on the Fujita scale (Fujita, 1971) based on the observed destruction (Barreiro et al., 2016). Remarkably, less than four years earlier on 6 December 2012, Dolores was struck by another large tornado. Though less impactful than the 2016 tornado, the 2012 tornado was also responsible for considerable damage on the outskirts of the town. A noteworthy description of both tornadoes is given in Fig. 2, which shows still frames from videos recorded from the very same location as the tornadoes hit the town.

The occurrence of two significant tornadoes in Dolores stresses the need to further document tornado events in Uruguay and, more generally, in SESA. It also raises a number of questions: What are the similarities and differences between the tornadoes occurring in 2012 and 2016? How do the meteorological conditions leading up to the two events compare, given that they occurred in different seasons (the 2012

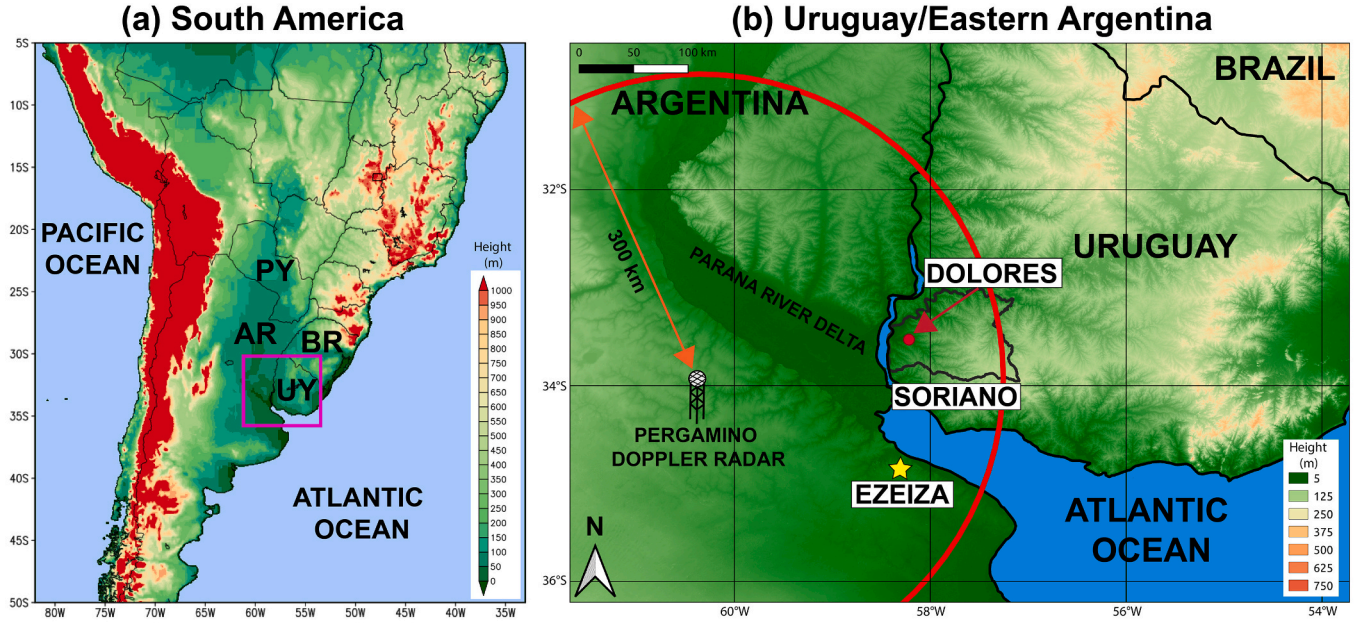

Fig. 1. (a) Terrain height (shaded; m) map of South America highlighting the countries of SESA (UY: Uruguay; AR: Argentina; BR: Brazil; PY: Paraguay) and main political borders (solid black lines). The magenta box denotes the enlarged area shown in (b). (b) Terrain height (shaded; m) map of Uruguay and eastern Argentina. The location of Dolores is represented by the red dot and the Department of Soriano is outlined in black. The Pergamino Doppler radar is denoted by the radar icon and its 300-km range ring is outlined in red. The yellow star indicates the location of Ezeiza. The Parana river delta is also annotated along its northern extent. (For interpretation of the references to colour in this figure legend, the reader is referred to the web version of this article.)

[1] Although the proliferation of cell phone cameras over the last two decades has greatly facilitated tornado reporting in SESA countries (Silva Dias, 2011; Salio et al., 2024).

Fig. 2. Select video frames of two strong tornadoes hitting the town of Dolores, Uruguay on 6 December 2012 (top) and 15 April 2016 (bottom). The dashed red arrows point to the same landmarks present in the top and bottom figures to show that both videos were filmed from the very same location. The top figure was rotated 10° clockwise for easier comparison with the bottom figure. The camera points to the southwest and the tornado moves to the southeast. The top figure is a courtesy of Edward Peña and the bottom figure is a courtesy of Arlington Perez. (For interpretation of the references to colour in this figure legend, the reader is referred to the web version of this article.)

and 2016 tornadoes took place in late spring[2] and mid fall, respectively)? Are there any common features in the synoptic- and mesoscale environments in these cases that may have influenced the formation and evolution of the tornadic storms? Addressing these questions is important to better understand the characteristics of tornadoes in the region, the environments that support them, and ultimately, provide more accurate forecasts and alerts for severe storm phenomena (e.g., Thompson and Edwards, 2000; Garner et al., 2021).

This study provides documentation and a detailed analysis of the Dolores tornado events of 6 December 2012 and 15 April 2016 based on the available information. Emphasis is given to the 2016 event, since it was more significant due to the damage it inflicted and was highly publicized due to the number of video recordings of the tornado as it struck Dolores. Moreover, evidence from environmental satellite imagery suggests that the tornado produced a damage track much longer than the original estimate that was based mostly on the damage reported in and around Dolores. The 2012 tornado case is analyzed and compared to the 2016 event. The comparison aims to establish similarities and discrepancies between the events on multiple scales and determine what can be learned from these cases to aid prediction of tornadoes in SWUY. Lastly, the analysis presented herein aims to highlight relevant aspects of the tornadic events that are of interest to future numerical studies.

The rest of this paper is organized as follows. Section 2 describes the datasets utilized in our analyses. Section 3 presents the results with emphasis on the multiscale aspects of the tornado events and comparisons between them. Conclusions are provided in Section 4.

2. Data

2.1. Operational meteorological data

Surface observations are rather sparse in SWUY thus being too coarse to adequately sample mesoscale features that may have influenced the formation and evolution of the Dolores storms. This scenario is aggravated by the nonexistence of upper-air stations in Uruguay, with those available located over 250–300 km away in neighboring countries. For this reason, gridded model data from the National Center for Environmental Prediction (NCEP) Climate Forecast System version 2 (CFSv2; Saha et al., 2014) and the fifth generation reanalysis of the European Centre for Medium-Range Weather Forecasts (ERA5; Hersbach et al., 2020) are used to obtain a more detailed assessment of the environment conducive to the Dolores tornadoes. CFSv2 is an operational extension of the NCEP Climate Forecast System Reanalysis (CFSR; Saha et al., 2010) project, consisting of global gridded data available at 0000, 0600, 1200, and 1800 UTC [2100, 0300, 0900, and 1500 Local Standard Time (LST)], with 0.5° horizontal grid spacing and 37 isobaric levels from the surface to 1 hPa. The ERA5 data have finer temporal and horizontal resolution than CFSv2, with hourly data at 0.25° horizontal grid spacing and 37 isobaric levels. Analyses based on both datasets are discussed in section 3c due to discrepancies in their representation of the pre-storm subsynoptic-scale environment in SWUY, as noted in other studies on severe storms in SESA which examined both datasets (Oliveira et al., 2022a; Ferreira et al., 2022). We point out in advance that the analysis of the synoptic-scale fields for both cases is carried out based on the CFSv2 analyses because they are clearly more consistent with an environment supportive of tornadic supercells for the 2016 event, while both CFSv2 and ERA5 show moderate performance in representing the near-storm environment in the 2012 case. A more general, in-depth comparison of the performance of CFSv2 and ERA5 in representing tornado and severe storm environments in SWUY is outside the scope of this article.

Analyses of the pre-storm mesoscale environment and the cloud-top features of the Dolores storms are carried out using the visible and thermal infrared channels of the Geostationary Operational Environmental Satellite 13 (GOES-13) over SWUY. We supplement the information provided by GOES-13 using surface station observations from SYNOP codes and hourly aviation routine weather reports (METARs) within 15 min of the satellite images selected for analysis. Despite the absence of Doppler weather radars within Uruguay, the early evolution of the 2016 Dolores supercell was observed by the Pergamino C-band (5.4-cm wavelength) Doppler radar, located in the province of Buenos Aires in eastern Argentina, approximately 130 km southwest of the initiation location of the supercell and 220 km southwest of Dolores, respectively. In spite of the long distance from the radar, relevant features of the early convection leading up to the 2016 Dolores supercell can be identified. For the 2012 case, however, analyses of the available radar data did not highlight any relevant feature of the storm; as a result, only GOES-13 imagery is used to analyze the evolution of the storm. In 2016, the Pergamino radar operated at single polarization, completing full volume scans every 10 min including plan position indicators (PPIs). Other relevant radar features include a range spacing of 480 m, maximum range of 480 km and a beamwidth of 0.98°.

2.2. Medium- and high-resolution satellite imagery

Most locations affected by the Dolores tornadoes encompassed rural and forested areas. Consequently, very few damage indicators were available for the two events outside the town. To estimate the extent of the damage tracks produced by the Dolores tornadoes, surface vegetation changes were subjectively inspected and mapped using Landsat-7 and Landsat-8 imagery from the U.S. Geological Survey (USGS) before and after the tornadoes using the closest cloudless days as done by Lopes

[2] Equivalently, during the early meteorological summer.

and Nascimento (2020). Landsat-8 employs its Operational Land Imager (OLI) to obtain 30-m resolution imagery in eight spectral bands and 15-m resolution imagery in its panchromatic band with a revisit period of 16 days. The closest cloudless day available before the 15 April 2016 tornado was 24 February 2016 while the closest cloudless days after the tornado were 21 April 2016 and 7 May 2016. The significant change in surface reflectance caused by tornadic winds through forest and crops facilitated the identification of the tornado track, except for short grass areas where tornado damage could not be detected. For the 2012 tornado, part of its damage track was identified through Landsat-7 imagery obtained on 21 December 2012. However, the Enhanced Thematic Mapper Plus (ETM+) imager aboard Landsat-7 malfunctioned and generated gaps in the images (Chen et al., 2011) which compromised the analysis of the damage track. The ETM+ sensor operates at eight spectral bands with a resolution of 15-m and one panchromatic band with a resolution of 30 m.

To obtain a more detailed view of the damage caused by the 2016 tornado, additional visible channel satellite imagery was obtained from Google Earth and inspected for the two closest cloudless days after the tornado (28 April and 13 May 2016). A similar analysis using Google Earth imagery for the 2012 event did not show significant (or even discernible) damage and is therefore not presented.

2.3. Visual observations and damage analysis

As the tornado impacted Dolores on 15 April 2016, numerous videos were taken by local residents. Because many of the videos were taken simultaneously and from different vantage points, a few selected ones are inspected herein since they provide an opportunity to analyze the early evolution and complex structure of the tornado during its intensification stage as it traversed the town. Similarly, videos of the 6 December 2012 tornado were also taken as the tornado crossed the outskirts of the town. Though only a few videos of this tornado were taken, they offer insight into some relevant features of the tornado and differences from the 2016 event. In addition, in situ photographs and videos of the damage produced by the tornadoes are used to obtain a rough estimate of their intensities.

3. Results

A number of key similarities and discrepancies exist between the 2012 and 2016 tornado cases. In order to compare the events and emphasize their most relevant features, we first present an analysis of the damage track and visual characteristics of each case separately followed by a multiscale analysis of their atmospheric environments. The analysis of the storm environment seeks to reveal, based on the limited observations available, synoptic and mesoscale features which played crucial roles in favoring tornado occurrence on 6 December 2012 and 15 April 2016 and which may be of relevance for severe storm development in SWUY.

3.1. The Dolores tornado cases

3.1.1. Damage track and visual observations of the 15 April 2016 tornado

Fig. 3 shows the track of the Dolores tornado based on the combined analysis of satellite-detected surface changes, damage reports, and visual observations. The tornado formed just west of Dolores and moved eastward during its early stages and then east-southeastward through most of its track. Videos of the tornado as it struck Dolores show that it quickly intensified and evolved into a “wedge”-shaped structure (Fig. 3b). Such rapid intensification resulted in significant damage early in the tornado’s track in west Dolores where the tornado completely collapsed warehouses and damaged numerous houses (mostly by removing their roofs and collapsing a few outer walls). The most severe damage occurred in downtown Dolores where the tornado downed unreinforced masonry walls of a number of houses, shops, and churches (Fig. 3c). Such damage would be consistent with an F3/EF3 tornado (Fujita, 1971; McDonald and Mehta, 2006). In addition, the widest portion of the tornado damage track was found in Dolores, estimated at 800 m based on surface damage reports.

As the tornado strengthened through Dolores, its structure changed considerably. The condensation funnel tilted toward the direction of motion of the tornado, a feature that is typically observed in fast-moving tornadoes (e.g., Knupp et al., 2014) and noted in videos of the Dolores tornado. A more interesting feature of the tornado, however, was the presence of horizontal vortices during the mid and late portion of its track through the town (Fig. 4). Horizontal vortices have been documented in a number of tornadoes, perhaps more prominently in intense, relatively fast-moving tornadoes with some forward tilt (Knupp et al., 2014; Houser et al., 2016; Bai et al., 2017; Oliveira et al., 2019). High-resolution radar observations and numerical simulations have suggested that these vortices emanate from the turbulent flow of a rear-flank downdraft (RFD) where surface friction and baroclinity enhance horizontal vorticity generation near the ground and around tornadoes (Houser et al., 2016; Bai et al., 2017; Oliveira et al., 2019, 2022b). Horizontal vortices have been documented in some instances to develop during intensification phases of tornadoes along small-scale convergence boundaries where the vortices are accumulated and subsequently tilted and stretched around the tornado (Houser et al., 2016; Bai et al., 2017; Oliveira et al., 2019, 2022b). Thus, the occurrence of horizontal vortices in the tornado as it traversed Dolores is consistent with its strengthening phase and may be an indication of unobserved small-scale storm processes participating in the intensification of the tornado.

East of Dolores and through the remainder of the tornado track, documentation of tornado damage at ground level became very scarce because most areas affected by the tornado were sparsely distributed farmlands and forested areas. Nevertheless, evidence of tornado damage in these areas was apparent on satellite data. Damage assessed on Google Earth imagery indicates that the tornado remained strong upon exiting Dolores and likely strengthened even further. Roughly 10 km southeast of Dolores, ground scouring was noted immediately downstream from a farmhouse (Fig. 3d) in a similar fashion to the type of damage shown in fig. 4 of Atkins et al. (2014) caused by a violent tornado on 20 May 2013 in Moore, Oklahoma. Ground scouring may be an indication of extreme wind speeds at the ground and is often observed in damage tracks caused by some violent tornadoes (Fujita, 1981, 1993; Knupp et al., 2014).

Farther southeast, Landsat-8 revealed that the tornado damage persisted over crops and open fields (Fig. 3e), ceased for approximately 10 km and then reappeared farther southeast in a forested area (Fig. 3f). In the region shown in Fig. 3f, the tornado track became non-contiguous, shifted from southeastward to northeastward, and narrowed. The abrupt narrowing of the damage track preceded its total cessation and implied tornado dissipation.

The causes of the gap in the tornado track are unclear, but two possibilities for it are discussed herein. First, it is possible that the tornado was actually on the ground continuously in this region but did not produce damage strong enough to be detected as surface changes on Landsat-8. If this is correct, then the total length of the tornado track is ~45 km. Second, it is possible that the supercell “cycled” in this region. Oftentimes, environments supportive of long-track tornadoes also support cyclic tornadogenesis, where the storm produces multiple tornadoes sequentially (Agee et al., 1976; Adlerman et al., 1999; Dowell and Bluestein, 2002; Knupp et al., 2014). In this scenario, the tornado that impacted Dolores would have had an estimated track length of ~30 km and its successor would have had a path length of at least ~5 km.

3.1.2. Damage track and visual observations of the 6 December 2012 tornado

Fig. 5 shows the estimated track of the 2012 Dolores tornado. Compared to the 2016 case, considerably less damage information is available for this tornado and it is mostly restricted to the town and its outskirts. The 2012 tornado also formed just west of Dolores and tracked

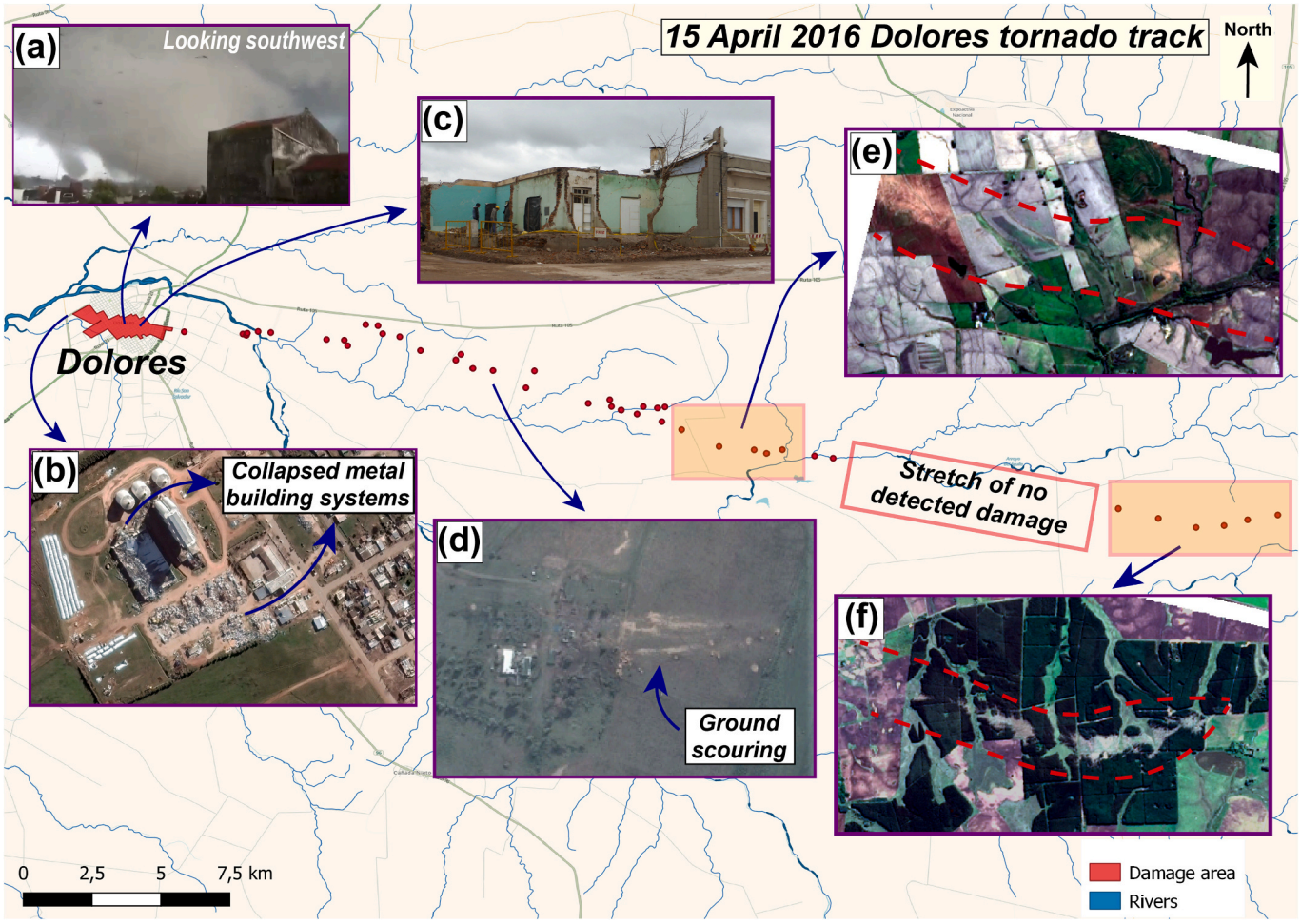

Fig. 3. Estimated track of the 15 April 2016 Dolores tornado. The red shaded area encompasses areas affected by the tornado in Dolores and red dots indicate more sporadic damage reports from rural regions southeast of the town. The blue arrows point to relevant features of the tornado discussed in the text such as (a) visual observations of the tornado, (b) significant damage to metal building systems, (c) F3/EF3 damage to houses near downtown Dolores, (d) evidence of ground scouring noted in Google Earth imagery, (e) tornado damage to crops and open fields, and (f) the end of the tornado track in a forested area. In the background, light gray and blue lines denote roads/streets and rivers, respectively. Figures (b,d) and figures (e,f) were obtained from Google Earth and Landsat-8, respectively. Figure (a) is a courtesy of Arlington Perez. (For interpretation of the references to colour in this figure legend, the reader is referred to the web version of this article.)

east-southeastward through the town slightly to the south of the 2016 tornado track (Fig. 5). The damage across the tornado track encompassed a broad area with relatively weak structural damage to houses, businesses, and vegetation with some embedded spots of more significant damage due to the large size of the tornado's parent circulation and its multiple-vortex structure (Fig. 5a; to be further discussed in the next paragraph). The most significant structural damage caused by this tornado includes roof removal of some houses and a gas station (Fig. 5b), overturning of agricultural machinery and storage containers (Figs. 5c, d). In general, such damage would be consistent with an F2/EF2 rating. Although visual observations of the tornado indicate that it persisted after exiting Dolores, no evident damage was found on Landsat-8 or Google Earth east of the town. Consequently, the available information is insufficient to determine the extent of the tornado track.

Videos of the tornado through Dolores show a rapidly rotating cloud base, which included a broad low-level mesocyclone and a concentrated area of lowered cloud and vertical vorticity (Fig. 6), the latter often termed "tornado cyclone" (e.g., Agee et al., 1976). Within the tornado cyclone, several large condensation funnels formed and dissipated intermittently while also revolving around each other. On several occasions, two or more occurred simultaneously. The structure exhibited by the 2012 tornado was composed of broad, strong low-level rotation and accompanied by the intermittent large multiple vortices reminiscent of the multiple-vortex mesocyclone (MVMC) structure discussed by Wurman and Kosiba (2013). This feature was also noted in other significant tornadoes (Wurman et al., 2014), including one in southern Brazil (Ferreira et al., 2022). This structure is also consistent with the broad swath of relatively minor damage through south Dolores with embedded areas of concentrated damage shown in Fig. 6. The observation of such a distinctive tornado structure in comparison to that displayed by the 2016 tornado likely reflects the impact of differences between the storm environments leading to the tornadoes that translated into distinct tornado morphologies and dynamics.

3.2. Synoptic-scale environments

We now evaluate the synoptic-scale environment that supported the Dolores tornadoes based on CFSv2 reanalysis data. The upper-level (250-hPa) flow in central South America at 1800 UTC (1500 LST) 15 April 2016 was characterized by a broad northwesterly jet stream crossing Andes Mountain range associated with a migratory trough in the westerlies and an anticyclone in central Brazil (Fig. 7a). The trough had split into two wave segments upon interacting with the Andes; a slower-moving trough upstream of the Andes (outside of the western domain boundary in Fig. 7a) and a faster-moving trough south of 40°S, which had begun to move across south South America. The northern

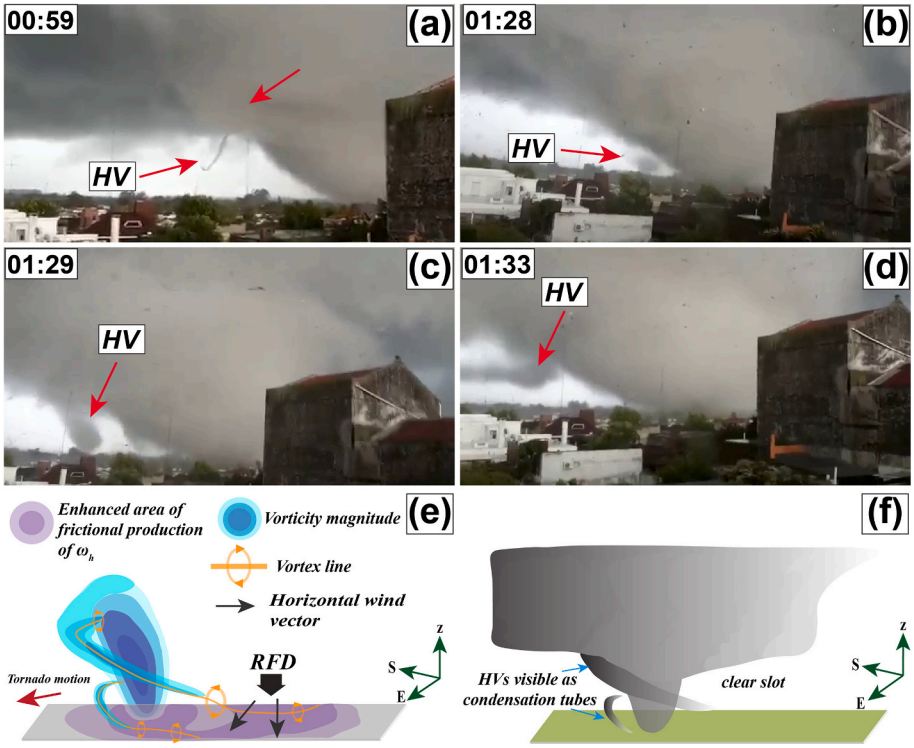

Fig. 4. Selected frames from a video of the 15 April 2016 tornado during its early intensification phase through Dolores, denoting relevant features of the tornado. Horizontal vortices (HVs) are indicated by red arrows with numbers 1–3 denoting the chronological order in which the HVs appear in the video. In all figures, the camera points to the southwest and the tornado moves to the southeast. Time stamps in the upper-right corner of each panel (minute:second) are relative to the beginning of the video. The video from which the panels are extracted is provided as Supplementary Video S1. Video and images courtesy of Arlington Perez. (e)–(f) Schematic of the evolution of HVs near tornadoes adapted from Oliveira et al. (2019) to a Southern Hemisphere cyclonic tornado. In (g), the three-dimensional (3D) vorticity field with a fast-moving, forward-tilting tornado with HVs wrapping around it (blue), with vortex lines indicating the sense of rotation of the HVs (orange), and zones of frictionally enhanced horizontal vorticity around the tornado (purple) in the tornado's outer flow and rear-flank downdraft (RFD; shown as downward-pointing thick black arrow) surrounding the tornado (indicated by the black arrows). In (h), the cloud field associated with the 3D vorticity field shown in (g) and consistent with the observations in (a)-(f). (For interpretation of the references to colour in this figure legend, the reader is referred to the web version of this article.)

flank of the 250-hPa jet extended into SWUY with wind speeds ~30–35 m s^{-1} and contained negligible divergence (and implied ascent) in that area, which is not surprising since this area was closer (but northward of) of the equatorward exit region and descending branch of the jet streak (Uccellini and Johnson, 1979; Rose et al., 2004; Bluestein et al., 2015). The flow structure at 500 hPa was generally similar to the 250-hPa flow, with wind speeds in the 25–30 m s^{-1} range in SWUY, and displayed no discernible short-wave disturbances that could have locally enhanced ascent (Fig. 7c). Overall, the mid- and upper-level winds were northwesterly and strong across SWUY and lacked substantial forcing for ascent during the afternoon. The long distance to the axis of the upstream upper-level trough placed SWUY far from quasi-geostrophic upward motion due to differential cyclonic vorticity advection, a scenario noted for other tornado events in SESA (Oliveira et al., 2022a; Ferreira et al., 2022; Veloso-Aguila et al., 2023; Lopes and Nascimento, 2024).

The 850-hPa flow was characterized by a strong (20–25 m s^{-1}) northwesterly low-level jet stream (LLJ; Salio et al., 2002; Marengo et al., 2004; Oliveira et al., 2018; Montini et al., 2019; Sasaki et al., 2022), stretching from the southern Amazon basin through Uruguay and into the southwestern South Atlantic Ocean (Fig. 7e). The presence of such a strong LLJ in the afternoon of 15 April 2016 was the result of an intense southwesterly-northeasterly height gradient between the northwestern Argentinean low (NAL; Seluchi et al., 2003) downstream of the upper-level trough and the South Atlantic high. The position and the core of the LLJ was shifted toward south Uruguay under the nose of the upper-level jet streak presumably due to the coupling between the upper- and low-level jets (Uccellini and Johnson, 1979; Saulo et al., 2007) and just north of a surface warm front (Ribeiro et al., 2016). The advection of warm and moist air from the Amazon basin by the LLJ promoted a broad zone of high equivalent potential temperature (θ_e) across western Uruguay and northeastern Argentina where the Dolores storm later developed.

The upper-level flow setup at 1800 UTC 6 December 2012 shared a number of similarities with the 15 April 2016 tornado event. At 250-hPa, a broad area of northwest-southeast-oriented strong wind speeds encompassed east-central Argentina and Uruguay due to two merging jet streaks, with the westernmost jet accompanying a positively tilted trough traversing the Andes and the easternmost jet in the far southern fringe of an anticyclonic circulation in Paraguay (Fig. 7b). This flow structure placed SWUY well under a divergence zone[3] and wind speeds ~20–30 m s^{-1}. The trough at 500 hPa was broader than its 250-hPa counterpart, but was nonetheless far upstream of SWUY at the time of tornado occurrence (Fig. 7d). Perhaps the most important feature of the 500-hPa flow was the establishment of 25–30 m s^{-1} winds (and associated deep-layer shear) over SWUY. Unlike the 2016 case, however, CFSv2 contains a short-wave vorticity minimum over SWUY that may have locally enhanced ascent and destabilization prior to the tornado. In summary, except for discrepancies in the jet and trough structures, the upper-level flow was northwesterly and strong on 6 December 2012 in SWUY around the time of the tornado as it was on 15 April 2016.

The main similarities between the 2012 and 2016 events lies in the 850-hPa wind fields. The intensity and structure of the northwesterly LLJ on 6 December 2012 was loosely similar to the 2016 event, but

[3] It should be pointed out, however, that some of the divergence noted in SWUY may be a result of CFSv2-parameterized convection from the early MCS.

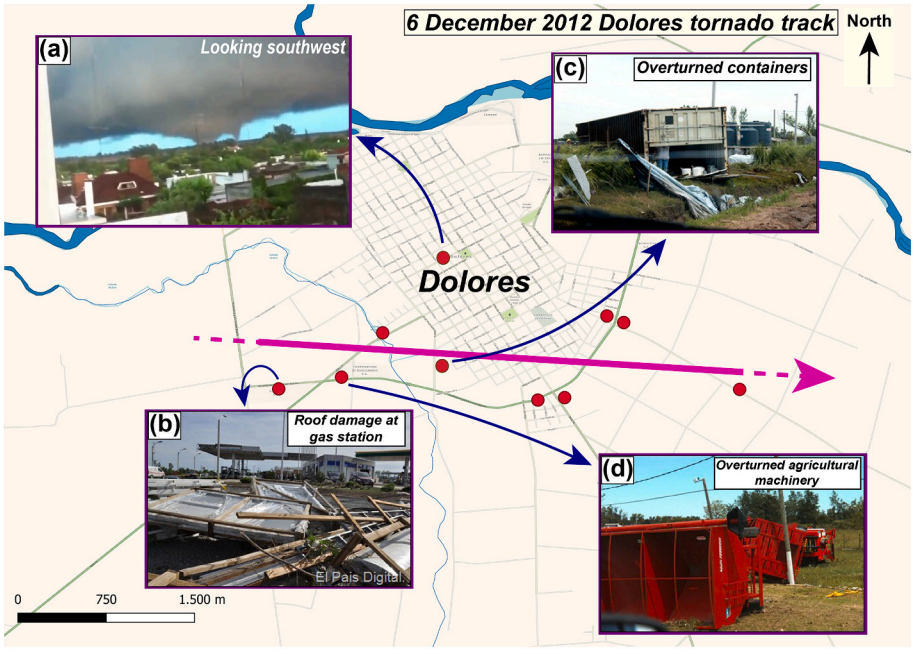

Fig. 5. Estimated track of the 6 December 2012 Dolores tornado. The red dots indicate damage reports in Dolores and outskirts and the magenta arrow denotes the approximate direction of the tornado track, with dashed segments indicating areas of uncertainty where the tornado began and moved toward. The blue arrows point to relevant features of the tornado discussed in the text such as (a) visual observations of the tornado, (b) roof removal of a gas station, (c) overturned metal containers, and (d) overturned agricultural machinery. In the background, light gray and blue lines denote roads/streets and rivers, respectively. Figures (b-d) are from blog Estacion bcp (http://bcpsalto.blogspot.com/2012/12/81112-tornado-en-dolores-inundaciones.html). Figure (a) is a courtesy of Edward Peña. (For interpretation of the references to colour in this figure legend, the reader is referred to the web version of this article.)

somewhat weaker near Dolores with ~15–20 m s^{-1} wind speeds (Fig. 7f). Nevertheless, different from the 2016 case, the LLJ was associated with a horizontal height gradient in the warm sector of a deepening trough (stretching from the NAL) which extended toward the coast of Argentina and Uruguay in response to the approaching upper-level trough. This flow configuration was associated with surface frontogenesis just in central Argentina and strong advection of high-θ_e air into SWUY and toward a warm front in southern Uruguay (Fig. 7h).

3.3. Mesoscale features, storm formation, and early evolution

A broad area of shallow and deep-layer cloudiness overcast much of SWUY and eastern Argentina on the morning of 15 April 2016. GOES-13 visible imagery at 1438 UTC (1138 LST) (Fig. 8a) shows a northwest-southeast-oriented band of low-level stratus clouds associated with warm advection by the LLJ in eastern Argentina and a mesoscale convective system (MCS) at the Uruguay-Argentina border and into SWUY in the vicinity of the warm front, which developed from a cluster of storms at the exit region of the LLJ during the previous night. Such a scenario is typical of SESA convective environments, where nocturnal MCSs form in the La Plata basin in association with low-level convergence and warm advection at the exit region of LLJs (Salio et al., 2007; Saulo et al., 2007; Oliveira et al., 2022a). A few robust storms were embedded in the morning MCS as noted in the Pergamino Doppler radar lowest PPI (Figs. 9a,b). Overall, the MCS moved to the southeast during the day.

The formation and early evolution of the Dolores supercell seem to have been influenced by the morning MCS. As the MCS moved into south and southeastern Uruguay by 1638 UTC (1338 LST), the air mass in its wake showed signs of rapid recovery noted by an increasing field of shallow cumulus convection (Fig. 8b). This recovery was fostered by low-level warm advection by the strong LLJ and unimpeded insolation due to rapid reduction of upper-level cloudiness transported downstream by the strong upper-level winds (Fig. 7a and c). Fig. 8a also shows an area of low-level stratus clouds with northeast surface winds and nearly saturated conditions in the wake of the MCS. GOES-13 suggests that this area destabilized at a slower rate during the afternoon early in comparison to the air mass just to its west; this is noted by a slow transition to stratus clouds to clear skies (Fig. 8b) and later into shallow cumulus (Fig. 8c) while the adjacent air mass to its west rapidly evolved into a deepening cumulus field (Figs. 8b,c) (this feature is more easily visualized in Supplementary Animation S1). Thus, based mostly on GOES-13 imagery, we speculate that a subtle outflow boundary may have been present just to the west of SWUY during in the few hours preceding the formation of the Dolores storm. A focused area of deepening cumulus clouds and "showers" can be noted in Figs. 8b,c and Fig. 9c, respectively, along the northern periphery of the Parana river delta. The presence of this deepening cumulus field and its northwest-southeast orientation along the delta may be an indication of enhanced low-level convergence amid a rapidly warming boundary layer. In fact, the Pergamino radar data at 1820 UTC (1520 LST) (Fig. 9c) shows a northwest-southeast zone of scattered echoes (reflectivity ~30–50 dBZ) developing and expanding at the intersection of the edge of the river delta. Given the existence of this line of cumulus clouds along the river delta and a possible outflow boundary from previous convection in the area where the Dolores storm formed later, we speculate that mesoscale convergence at the northern periphery of the Parana river delta possibly augmented by an outflow boundary may have participated in the initiation of the convection that evolved into the Dolores storm.

The echo associated with the Dolores storm emerged from the deepening cumulus field between 1820 UTC (Fig. 9c) and 1835 UTC (Fig. 8c) in eastern Argentina, approximately 100 km west-northwest of Dolores. The storm tracked southeastward and remarkably strengthened as noted in the rapid expansion of its anvil and the development of a persistent overshooting top (Fig. 8c–e), both features indicative of very strong updrafts (Bluestein et al., 2019; Borque et al., 2020). Later, during evening hours, enhanced thermal infrared imagery (Fig. 8f) shows that the supercell remained strong after dark, with cloud top brightness temperatures (T_B) < −90°C. After 2035 UTC (Fig. 8f), except for some

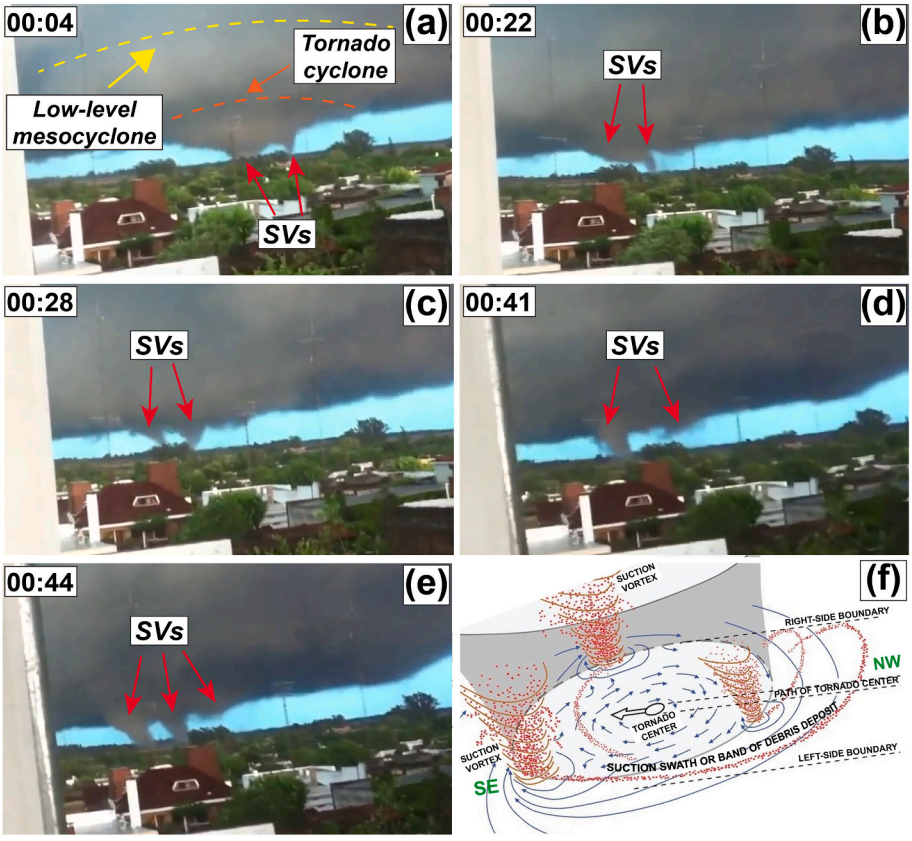

Fig. 6. Selected frames from a video of the 6 December 2012 tornado as it tracked through the outskirts of Dolores, denoting relevant features of the tornado. Suction or subvortices (SVs) are indicated by red arrows. In all figures, the camera points to the southwest and the tornado moves to the southeast. Time stamps in the upper-right corner of each panel (minute:second) are relative to the beginning of the video. The video from which the panels are extracted is provided as Supplementary Video S2. Video and images courtesy of Edward Peña. (h) Schematic of the evolution of multiple vortices in a tornado adapted from Wakimoto et al. (2022) (© American Meteorological Society. Used with permission) to a Southern Hemisphere cyclonic tornado. The flow around the tornado and its subvortices is represented by curved streamlines/arrows and debris lofted by the subvortices and deposited in streaks at the surface are denoted by red dots. The gray shading denotes the cloud field associated with the parent tornado and its subvortices. (For interpretation of the references to colour in this figure legend, the reader is referred to the web version of this article.)

semi-discrete trailing convection in the flanking line of the Dolores supercell (Fig.s 9e,f), the coldest T_B of the storm anvil merged with other anvils downstream that were associated with the remnants or redevelopment of the morning MCS downstream.

The mesoscale setup of the 2012 tornadic supercell shares a number of important similarities to the 2016 event. During the morning of 6 December 2012, an expansive cloud shield from a nocturnal MCS encompassed much of Uruguay ahead of a developing line of storms along a slow-moving cold front in eastern Argentina (Fig. 10a). As the MCS moved rapidly to the southeast during the early afternoon, it established an outflow boundary approximately 80 km west of the border between eastern Argentina and SWUY (Fig. 10b) and a broken field of low-level stratus in SWUY. In spite of the low-level cloud cover, sufficient insolation fostered by persistent warm-air advection by the LLJ was capable of destabilizing the atmosphere in the area (Fig. 10c).

An outflow boundary from the morning MCS is clear in this event as a semi-circular line of cumulus clouds that extended from northern Uruguay into eastern Argentina (Fig. 10b) separating warmer temperatures (30–37°C) on its west side in Argentina from cooler temperatures on its east side (25–30°C) in SWUY. The boundary retreated to the east closer to the Argentina-Uruguay presumably due to the strong low-level northwesterly winds (Fig. 10c–e). In addition, from early to mid-afternoon, persistent lines of cumulus clouds developed in the vicinity and parallel to the Parana river delta and ahead of deep convection at the cold front (Fig. 10c–e) (both the outflow boundary and the lines of cumulus clouds are more easily noted in the Supplementary Animation S2). As with the 2016 event, based on the available GOES-13 imagery and surface data, we speculate that the initiation of the Dolores storm of 2012 may have been aided by convergence at the northern edge of the Parana river delta possibly enhanced by an interaction with the outflow boundary just west of SWUY.

Upon crossing the border and impacting Dolores, GOES-13 visible imagery shows that the storm's updrafts strengthened significantly (Fig. 10e–f) by developing a broad anvil and vigorous overshooting top. The supercell persisted well after striking Dolores and through the evening, maintaining cloud top $T_B < -90$°C. After 2128 UTC, the anvil of the supercell merged with anvils from the storms at the approaching cold front and, eventually, the storm was absorbed into a developing MCS (Figs. 10f).

3.4. Model-derived profiles and convective parameters

A common issue in severe storm studies in SESA is the rarity of proximity soundings, a result of the sparse upper-air network in South America and the lack of operational soundings during the afternoon representative of pre-convective conditions near the time of the strongest surface heating (Nascimento et al., 2016; dos Santos et al., 2023). As a result, case studies (Nascimento et al., 2014; Oliveira et al., 2022a; Ferreira et al., 2022) and climatologies of severe storms in SESA (Brooks et al., 2003; Nascimento et al., 2016; Piscitelli et al., 2022; dos Santos et al., 2023; Veloso-Aguila et al., 2023; Lopes and Nascimento, 2024) have employed "pseudo" soundings extracted from global or regional

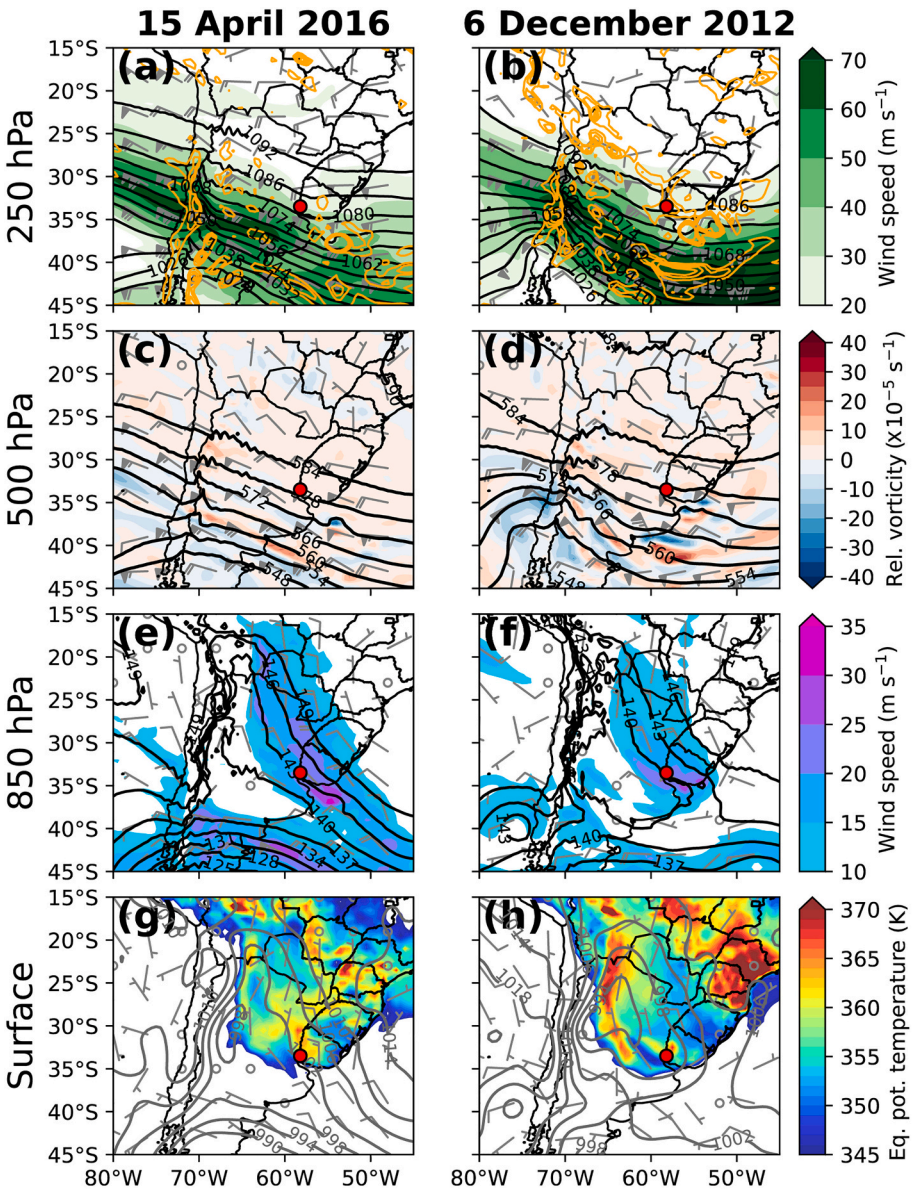

Fig. 7. CFSv2 synoptic fields for the (left column) 1800 UTC 15 April 2016 and (right column) 1800 UTC 6 December 2012 Dolores tornado cases (for reference, Local Standard Time LST = UTC - 3). (a,b) 250-hPa geopotential heights (dam; black contours), winds (m s^{-1}; barbs), and divergence ($\times 10^{-5}$ s^{-1}; orange contours every 2×10^{-5} s^{-1} starting at 2×10^{-5} s^{-1}). (c,d) 500-hPa geopotential heights (dam; black contours), winds (m s^{-1}; barbs), and relative vorticity ($\times 10^{-1}$ s^{-1}; shaded). (e,f) 850-hPa geopotential heights (dam; black contours), winds (m s^{-1}; barbs), and wind speed (m s^{-1}; shaded). (g,h) 2-m above ground level (AGL) equivalent potential temperature (K; shaded), pressure reduced to mean sea level (hPa; dark gray contours), and 10-m AGL winds (m s^{-1}; wind barbs). Black contours in the background denote South America and its geopolitical boundaries. Wind barbs depict the following: half barbs = 5 m s^{-1}; full barbs = 10 m s^{-1}; flags = 25 m s^{-1}. The red circle denotes the location of Dolores. (For interpretation of the references to colour in this figure legend, the reader is referred to the web version of this article.)

numerical model analysis to determine the vertical structure of the atmosphere preceding and during severe weather events. Using a similar methodology, we herein investigate model-derived soundings near the Dolores area for the 2012 and 2016 tornadoes using the CFSv2 and ERA5 global model datasets. The two datasets are evaluated in light of relevant discrepancies noted in these two events. First, we evaluate the performance of CFSv2 and ERA5 model profiles by comparing them with the nearest observed sounding in time and space to Dolores, located in Ezeiza, Argentina (SAEZ; location indicated in Fig. 1b), at 1200 UTC (0900 LST). It should be pointed out that gridded-model products such as CFSv2 and ERA5 represent, at best, crude estimates of the actual pre-storm environments in observation-sparse regions, such as SESA. Therefore, results for specific cases should be taken in a qualitative sense as a means to estimate the general magnitude and vertical distribution of convective ingredients conducive to supercell tornado development.

We begin our assessment of the model-derived profiles for the 2016 event (Fig. 11). Fig. 11a presents the 1200 UTC (0900 LST) 15 April 2016 SAEZ sounding while Fig. 11b and c present corresponding profiles taken at the closest grid points to Ezeiza from CFSv2 and ERA5 data, respectively. The main features of the SAEZ thermodynamic profile are (i) a shallow near-ground temperature inversion, (ii) a layer of steep lapse rate between 620 and 700 hPa under a thin inversion layer, and (iii) overall drying above 800 hPa. This structure results in a thick (950–700-hPa) layer with mean-layer convective inhibition (MLCIN) (−30 J kg^{-1}) and substantial mean-layer convective available potential energy (MLCAPE) (1900 J kg^{-1}) under an equilibrium level (EL) just below 150 hPa. The near-ground stable layer is a consequence of the diurnal cycle of the boundary layer and low-level cloud cover near the warm front discussed in section 3b while the relatively large CAPE is due to the steep lapse rate layer at mid levels. A generally similar

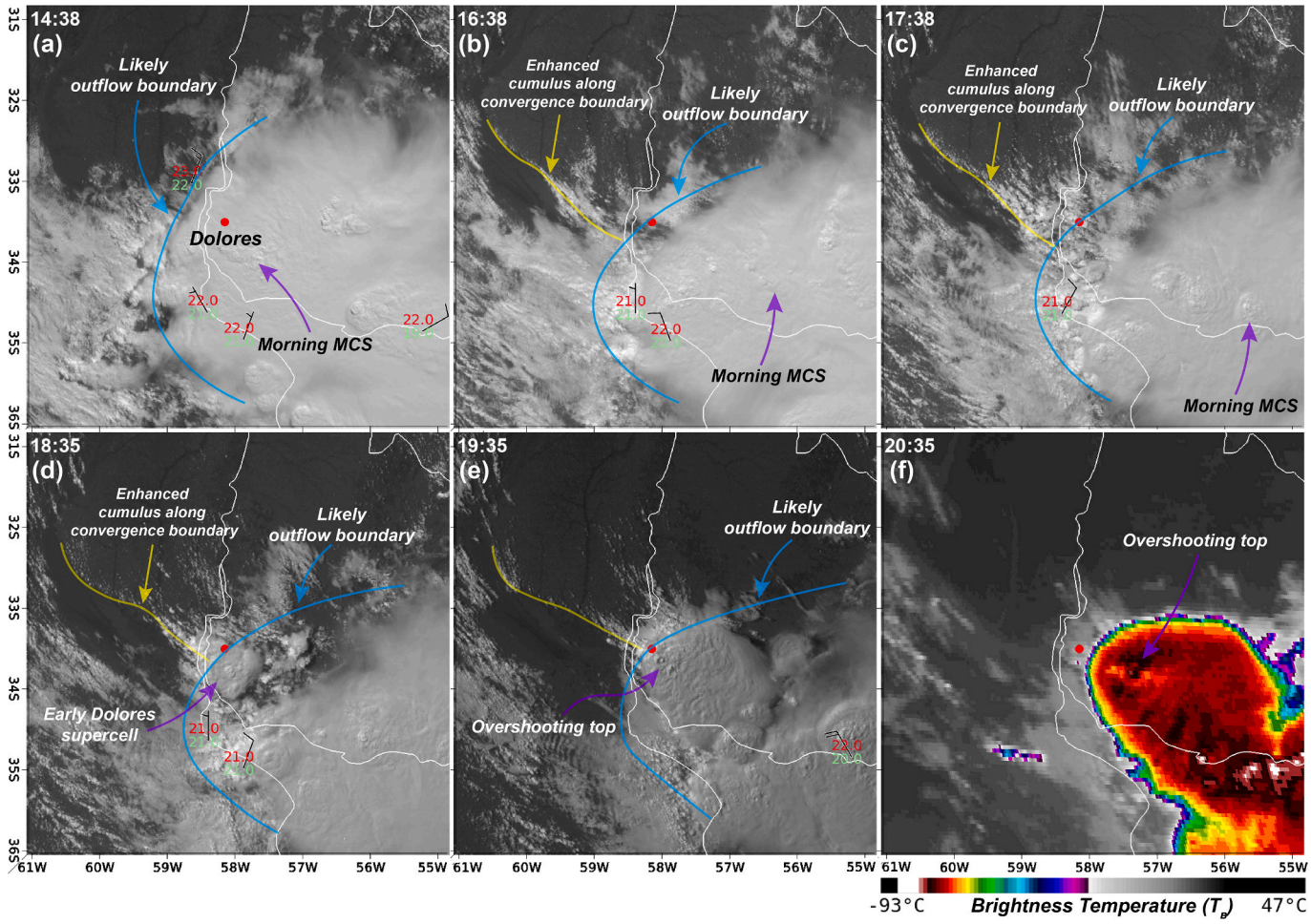

Fig. 8. GOES-13 imagery centered on SWUY on 15 April 2016. Visible imagery shown at (a) 1438, (b) 1638, (c) 1738, (d) 1835, and (e) 1935 UTC, and enhanced infrared imagery shown at (f) 2035 UTC (for reference, Local Standard Time LST = UTC - 3). Surface observations from SYNOP and METAR stations within 15 min of the satellite images are also shown and include temperature (red; °C), dewpoint temperature (green; °C), and wind (barbs; half barbs = 2.5 m s^{-1} and full barbs = 5 m s^{-1}). Boundaries associated with the Parana river delta and outflow from previous convection are outlined in yellow and blue, respectively. The red circle denotes the location of Dolores. (For interpretation of the references to colour in this figure legend, the reader is referred to the web version of this article.)

configuration is observed for the CFSv2 profile (Fig. 11b) with comparatively substantial CAPE, CIN, EL height, and drying atop the low-level moist layer. Nevertheless, CFSv2 underestimates the strength of the near-ground inversion and displays smoother mid-level lapse rates without a shallow inversion capping it. In addition, the depth of the moist layer in the CFSv2 extends to ~700 hPa against ~800 hPa in the SAEZ profile. In turn, the ERA5 profile (Fig. 11c) shows substantially less MLCAPE for any near-ground lifted parcel, lower EL height, and higher MLCIN than SAEZ and CFSv2 due to a deeper near-surface stable layer and warmer air in the 900–700 hPa-layer. Similar to CFSv2, the ERA5 profile does not have layers of steep lapse rate under a capping inversion at mid levels, which also results in nearly the same 700–500-hPa lapse rates seen in the CFSv2 profile. The depth of the moist layer in ERA5 falls in between the ones depicted in the SAEZ and CFSv2 profiles but the magnitude of the upper-level drying is underestimated, mainly above 500 hPa. Overall, CFSv2 depicts a thermodynamic profile that is somewhat closer to SAEZ.

Regarding the wind profiles, SAEZ displays long, counterclockwise-turning hodographs in the lower troposphere, consistent with warm advection by a LLJ (Fig. 11a). Both CFSv2 and ERA5 profiles (Fig. 11b and Fig. 11c, respectively) underestimate the length and easterly component of the winds near the surface and, consequently, depict weaker 0–1-km storm-relative helicity (SRH) (e.g., SRH1 of −190 and −185 m^2 s^{-2} for CFSv2 and ERA5, respectively, against −225 m^2 s^{-2} at SAEZ). Despite that, the general shape of the CFSv2 hodograph is similar to SAEZ throughout the troposphere. In contrast, ERA5 contains excessive counterclockwise turning of the midlevel winds. These differences result in much better estimates of the SAEZ-derived storm motion for left-moving (cyclonic) supercells for CFSv2 (15 m s^{-1}, the same value found at SAEZ) than ERA5 (11.0 m s^{-1}) and underestimates of the observed deep-layer shear [bulk wind difference over 0-6 km (BWD6) of 33 m s^{-1}] for both CFSv2 (29 m s^{-1}) and ERA5 (25 m s^{-1}). Hence, as with the thermodynamic profiles, CFSv2 provides a slightly estimate of the observed kinematic profile.

In light of the above comparison, we now assess the CFSv2 and ERA5 profiles valid at 1800 UTC (1500 LST) 15 April 2016 for the grid points closest to Dolores (Fig. 12), around 1 h before the tornado impacted the town. The CFSv2 thermodynamic profile (Fig. 12a) is consistent with an environment conducive to vigorous deep convection; it contains large MLCAPE (2500 J kg^{-1}) and small MLCIN (−10 J kg^{-1}), despite weak mid-level lapse rates. The robust MLCAPE and weak MLCIN denoted by CFSv2 are due to its warm, deep moist layer, which is mostly consistent with warming and moistening observed in the wake of the morning MCS discussed in section 3b. The ERA5 profile (Fig. 12b) is drastically different, marked by a persistent low-level stable layer which results in relatively small MLCAPE and large MLCIN, despite its slightly stronger mid-level lapse rates. In addition, the ERA5 profile has less midlevel drying, similar to the ERA5 morning profile at Ezeiza. In contrast to the CFSv2 profile, the more stable and less favorable environment for severe storms shown in the ERA5 data occurs in response to the spurious

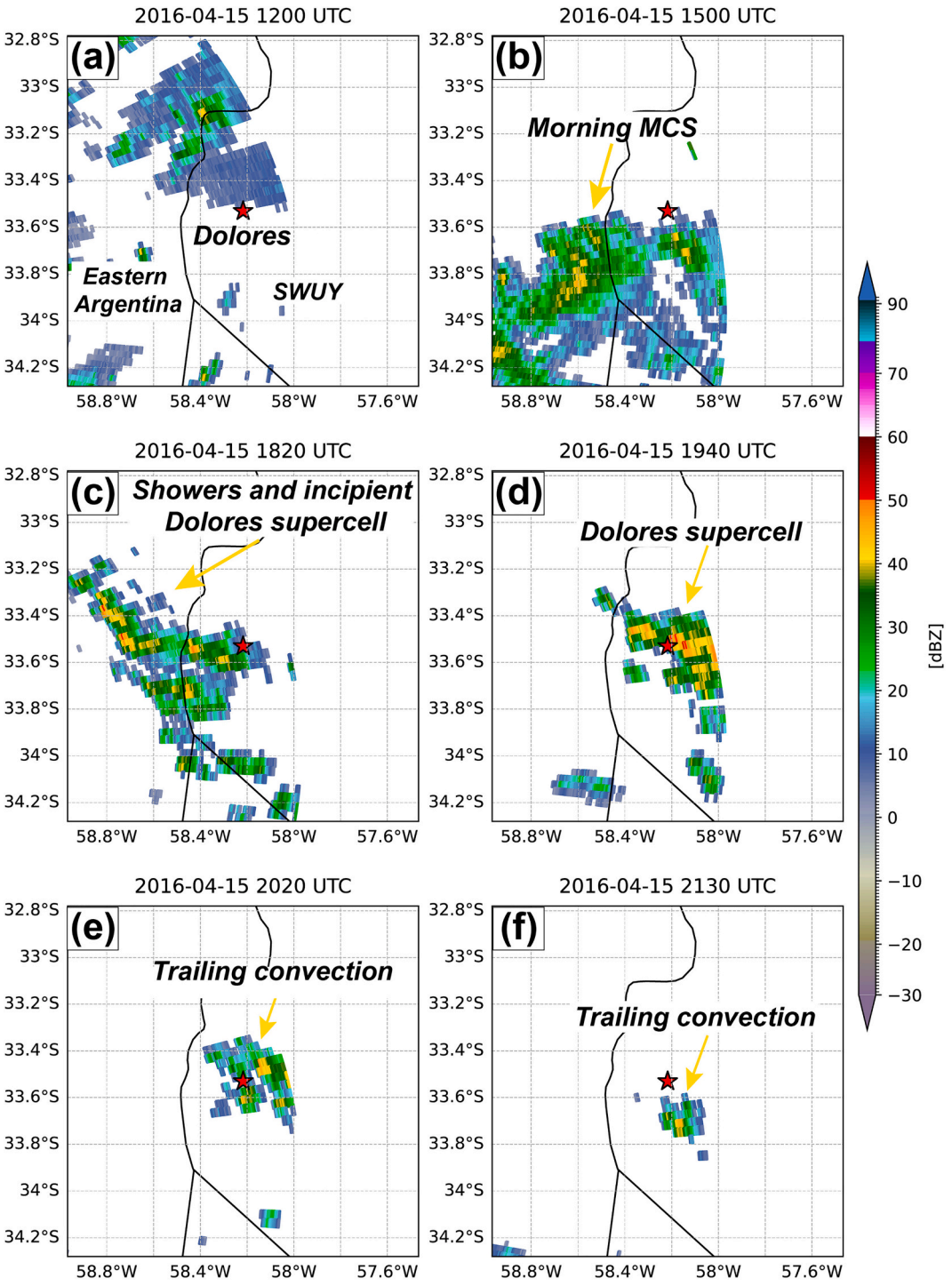

Fig. 9. Pergamino (Argentina) Doppler radar 0.5° plan-position indicator centered on SWUY and eastern Argentina on 15 April 2016 at (a) 1200, (b) 1500, (c) 1820, (d) 1940, (e) 2020, and (f) 2130 UTC (for reference, Local Standard Time LST = UTC - 3). The red marker denotes the location of Dolores. The echoes observed near Dolores are located above 6 km AGL. (For interpretation of the references to colour in this figure legend, the reader is referred to the web version of this article.)

persistence of a low-level cold pool from the morning MCS in SWUY, which is also responsible for a small jet-like flow within the stable layer (lower portion of the hodograph in Fig. 12b). This cold pool and attendant stability persist during the afternoon hours over much of SWUY (see Supplementary Figure S1).

The wind profile depicted by CFSv2 is also consistent with the occurrence of a strong tornado (Fig. 12a). The hodograph is long throughout the troposphere and contains BWD6 of 23 m s^{-1} which, coupled with robust CAPE, is rather favorable for supercells. Moreover, the presence of stronger shear over a deeper layer, herein measured as the bulk wind difference over 0–8 km (BWD8), of 30 m s^{-1} tends to favor the occurrence of long-lived supercells (Bunkers et al., 2006; Garner et al., 2021). In the low levels, the hodograph is also long and anticyclonically curved, containing ample SRH3 for mesocyclones (−230 m^2 s^{-2}) and near-ground SRH for strong tornadoes (SRH1 and SRH0–0.5 of −135 and − 95.0 m^2 s^{-2}, respectively; Rasmussen, 2003; Coffer et al., 2019). Such a large SRH occurs partially because of the fast storm motion for the left-moving supercell of 19 m s^{-1}, an estimate that is deemed

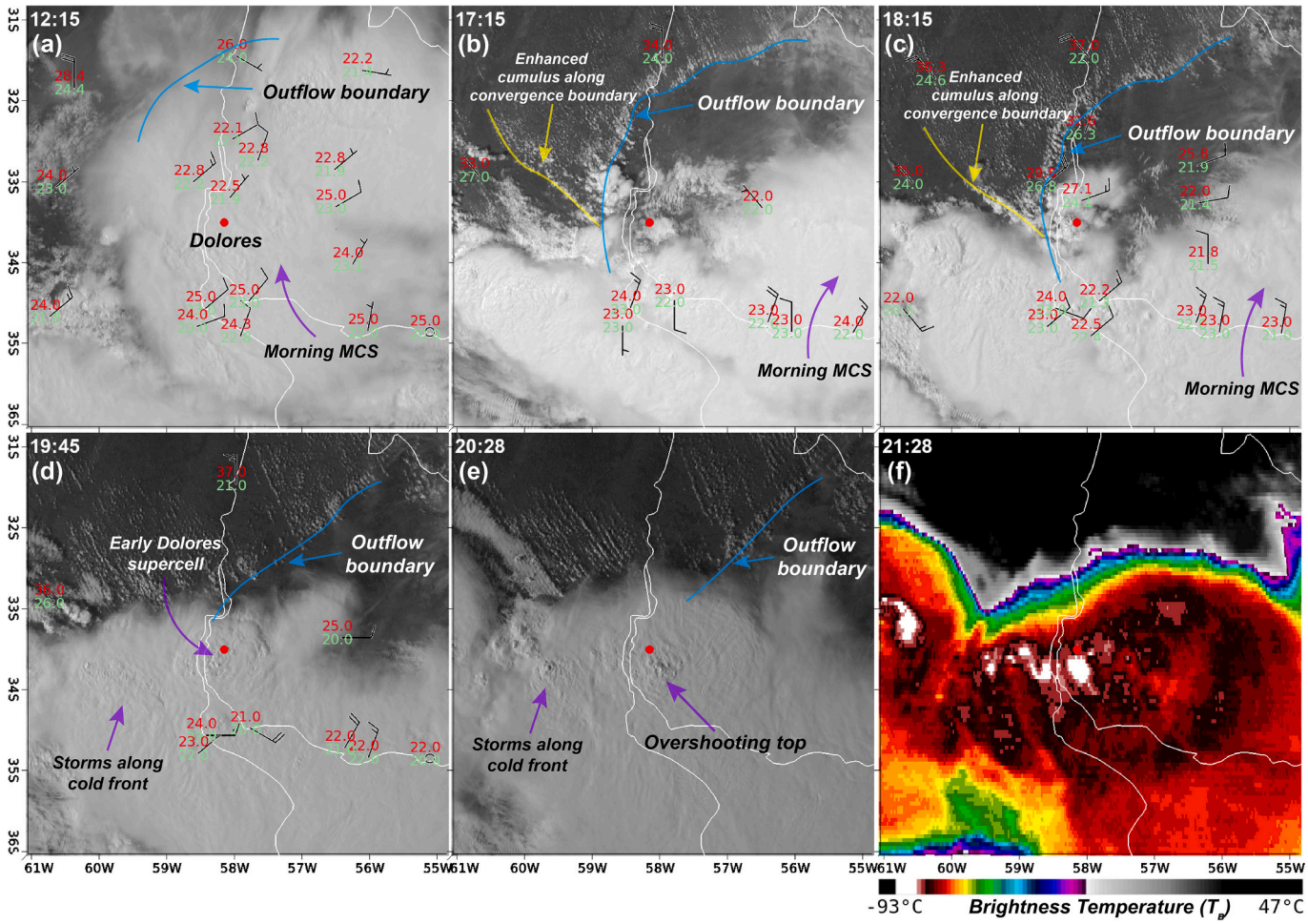

Fig. 10. GOES-13 imagery centered on SWUY on 6 December 2012. Visible satellite imagery shown at (a) 1215, (b) 1715, (c) 1815, (d) 1945, (e) 2028, and enhanced infrared imagery shown at (f) 2128 UTC (for reference, Local Standard Time LST = UTC - 3). Surface observations from SYNOP and METAR stations within 15 min of the satellite images are also shown and include temperature (red; °C), dewpoint temperature (green °C), and wind (barbs; half barbs = 2.5 m s^{-1} and full barbs = 5 m s^{-1}). Boundaries associated with the Parana river delta and outflow from previous convection are outlined in yellow and blue, respectively. The red circle denotes the location of Dolores. (For interpretation of the references to colour in this figure legend, the reader is referred to the web version of this article.)

reasonable given the previously discussed correspondence between SAEZ and the associated CFSv2 profile at 1200 UTC. Coupled with low mean-layer lifting condensation level (MLLCL) heights of 550 m, the CFSv2 profile therefore clearly depicts an environment supportive of long-lived supercells with the potential to produce strong, long-tracked tornadoes (Thompson et al., 2003, 2007, 2012; Garner et al., 2021). In contrast, a look at the ERA5 hodograph (Fig. 12b) indicates an environment with higher shear than CFSv2 over the troposphere. Nevertheless, much of this heightened shear occurs because of the spurious low-level cold pool producing a jet-like flow with a strong easterly component, thus augmenting the bulk wind differences in the shear computations.

We now assess the model-derived profiles for the 2012 case (Fig. 13). Unfortunately, for this event, the SAEZ 1200 UTC 6 December 2012 was prematurely terminated around 550 hPa (Fig. 13a) and only an assessment of the low-level environment around Ezeiza is possible. The main features of the low-level SAEZ thermodynamic profile include a (i) shallow near-surface temperature inversion, (ii) steeper temperature lapse rates and drier air above 850 hPa, and (iii) saturated air above 700 hPa. The CFSv2 and ERA5 profiles show notable similarities and discrepancies with the SAEZ profile (Fig. 13b and c). On one hand, CFSv2 has a shallow low-level stable layer comparable to that of SAEZ but lacks drying and steep lapse rates above 850 hPa and is saturated through a much deeper layer (880–650 hPa). On the other hand, as in SAEZ, ERA5 has steeper lapse rates above 800 hPa but contains a deeper, weaker low-level stable layer and drier air above 800 hPa, lacking saturation above 700 hPa. As for the low-level winds, SAEZ and the corresponding model profiles contain northeasterly jetlike flows around 1 km AGL influenced by the cold pool of the early MCS. The CFSv2 profile has a jetlike flow that is closer in magnitude to that of SAEZ and a similar pattern of veer-back-veer flow above 1 km AGL, while ERA5 underestimates the intensity of the jet and displays a straight hodograph above 1 km AGL. It seems the environment at Ezeiza at 1200 UTC 6 December 2012 may at best be slightly better depicted by CFSv2 than ERA5. From this analysis, we deem the model-derived environments depicted in the following paragraph at 1800 UTC to be less accurate than those discussed for the 2016 event and, as such, should be taken only as crude estimates of the actual environment leading to the 6 December 2012 tornado.

Keeping in mind the caveats noted above, the CFSv2 and ERA5 profiles at 1800 UTC 6 December 2012 for the grid points closest to Dolores around 2 h before the tornado are now evaluated in Fig. 14. The two thermodynamic profiles possess modest MLCAPE but the structures of the profiles are distinct. The CFSv2 is relatively drier below 700 hPa and above 620 hPa (except around 500 hPa) (Fig. 14a) than the ERA5 profile which, in turn, is saturated below 880 hPa (Fig. 14b). These differences result in lower MLCAPE, higher MLCIN and higher MLLCL height depicted by CFSv2. The presence of moderate MLCIN in both profiles is due to temperature inversion layer below 900 hPa in CFSv2

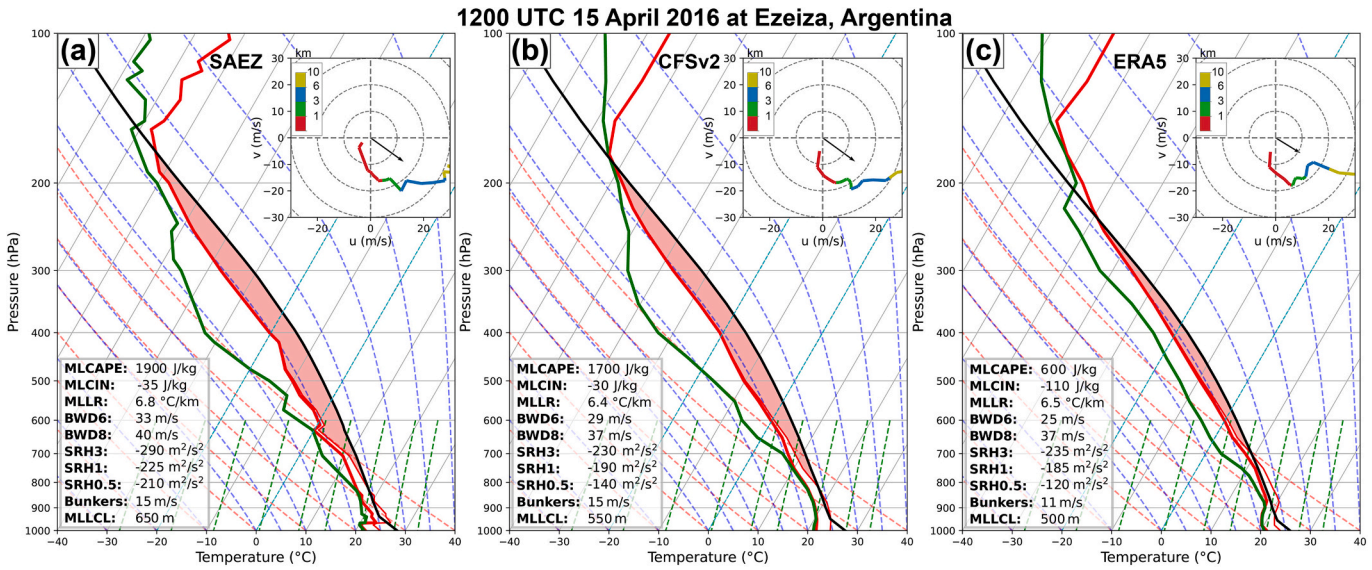

Fig. 11. Comparison of observed and model-derived thermodynamic and kinematic profiles plotted as Skew*T*-log*p* diagrams and hodographs (insets at the top-right corner of each figure), respectively, for the upper-air station closest to Dolores, Uruguay, located at Ezeiza, Argentina (SAEZ) at 1200 UTC (0900 LST) 15 April 2016. The observed SAEZ profiles are shown in (a) and the profiles from the grid points closest to Ezeiza from CFSv2 and ERA5 are shown in (b) and (c), respectively. In the Skew*T*-log*p* diagrams, the solid thick red, thin red, and thick green lines denote, respectively, the temperature, virtual temperature, and dewpoint temperature of the environment. The black solid line represents a mixed-layer-based parcel lifted pseudo adiabatically with the virtual temperature correction applied (Doswell III and Rasmussen, 1994). The semi-transparent red shaded area denotes the CAPE for a mixed-layer-based parcel. In the hodograph insets, the sfc-1 km, 1–3 km, 3–6 km, and 6–10 km AGL layers are colored in red, green, blue, and olive, respectively. The black arrow extending from the origin of the hodograph denotes the storm motion vector of a left-moving cyclonic supercell based on the Bunkers internal dynamics method (Bunkers et al., 2000). On the lower left corner of each plot, selected relevant convective parameters are presented: MLCAPE, MLCIN, 500–700-hPa lapse rate (MLLR), 0–6-km BWD (BWD6), 0–8-km BWD (BWD8), SRH3, SRH1, SRH0–0.5, magnitude of the Bunkers storm motion for left-moving supercells, and MLLCL heights. (For interpretation of the references to colour in this figure legend, the reader is referred to the web version of this article.)

and around 900 hPa in ERA5. The layer of higher stability and relative humidity in ERA5 is similar to the one discussed for the 1800 UTC 15 April 2016 ERA5 profile and is due to the spurious persistence of a cold pool from the morning MCS in SWUY (shown in the Supplemental Figure S1).

As with the thermodynamic profiles, the wind profiles from CFSv2 and ERA5 are very different. The CFSv2 hodograph is long, nearly straight in the 0–3 km AGL layer and veers from northwesterlies to westerlies above 3 km AGL (Fig. 14a). This hodograph, though able to support long-lived supercells (given its BWD8 of 28 m s^{-1} and SRH3 of -100 m^2 s^{-2}), is not the most typical type of hodograph associated with tornadic supercells, which often exhibit more low-level curvature and storm motion significantly off the hodograph (i.e., veering of the shear vector) (Klemp, 1987; Thompson et al., 2003; Veloso-Aguila et al., 2023; Lopes and Nascimento, 2024). This is reflected in the modest near-surface SRH depicted in Fig. 14a (SRH1 and SRH0–0.5 of -75 and -50 m^2 s^{-2}, respectively) due to the lack of observed northeasterly surface-winds near Dolores (Fig. 10c). In turn, the ERA5 hodograph is more consistent with an environment supportive of significantly tornadic supercells (Fig. 14b). It contains ample low-level curvature and storm motion that is well off the hodograph such that it is associated with SRH3, SRH1, and SRH0–0.5 of -235, -150, and -100 m^2 s^{-2}, respectively, in addition to large BWD8 (30 m s^{-1}). The larger SRH displayed by the ERA5 profile is in concert the observed surface northeasterly winds (Fig. 10c). As with the analysis of the 1800 UTC 15 April 2016 wind profiles, however, the higher shear in the ERA5 hodograph must be considered with caution because of the presence of spurious cold pool discussed above.

4. Summary and concluding remarks

This study presented a multiscale analysis of the 6 December 2012 and 15 April 2016 tornadoes that impacted the town of Dolores, in southwestern Uruguay (SWUY). Both tornadoes produced significant damage through the town, with the second tornado in 2016 being more severe and causing damage that extended several kilometers east-southeast of Dolores as observed in environmental satellite imagery. Videos of the 2016 tornado showed it grew quickly into a "wedge" morphology and exhibited horizontal vortices in its periphery, a feature that has been associated with other strong/violent tornadoes and may be an indicative of tornado intensification processes. In turn, videos of the 2012 tornado reveal that it developed within a broad, rapidly rotating mesocyclone with a multiple-vortex structure, a feature that seems reminiscent of multiple-vortex mesocyclones discussed in Wurman and Kosiba (2013) and Wurman et al. (2014), and believed to develop out of unstable vortex Rossby waves (Huang and Xue, 2023). The damage as well as the visual observations further highlight the significance of both tornado events and stress the need for more research on tornadoes in Uruguay. We point out that, despite being located in one of the most tornado-prone parts of SESA (Lopes and dos Santos, 2022), research focused on tornadoes in Uruguay remains scarce; in fact, to the authors' knowledge, our study is the first to provide a detailed assessment of tornadic supercell cases in Uruguay.

One of the main goals of this study was to compare the synoptic-scale environments that led to the 2012 and 2016 tornadic storms to determine any relevant similarities and differences between the cases. Indeed, it was found that the two events shared a number of synoptic-scale similarities even though the storms occurred in different seasons (the 2012 and 2016 tornadoes occurred in late spring and mid fall, respectively). Both storms developed far ahead of an upper-level trough near the Andes, under strong mid- and high-level winds and associated deep-layer shear. Because the tornadic supercells developed far from the main troughs, mid-level dynamic lifting thus did not seem to play a major role in setting up the severe storm environments, although short-wave troughs embedded in the flow may have locally enhanced lift in the 2012 case. At the surface, both supercells developed in a large warm

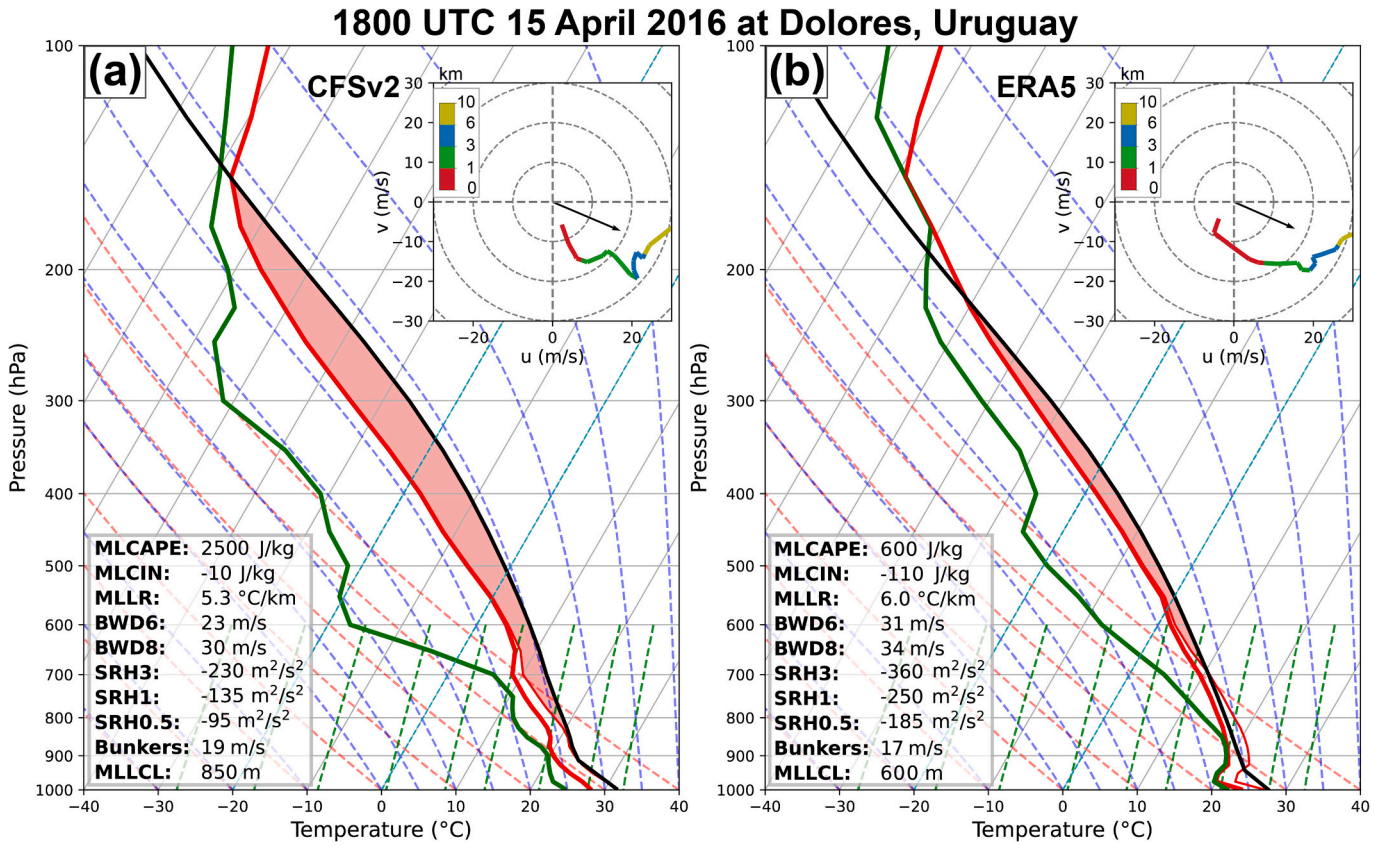

Fig. 12. Grid-point thermodynamic and kinematic profiles plotted as Skew*T*-log*p* diagrams and hodographs (insets at the top-right of each figure), respectively, from the grid points closest to Dolores, Uruguay, from (a) CFSv2 and (b) ERA5 at 1800 UTC (1500 LST) 15 April 2016. In the Skew*T*-log*p* diagrams, the solid thick red, thin red, and thick green lines denote, respectively, the temperature, virtual temperature, and dewpoint temperature of the environment. The black solid line represents a mixed-layer-based parcel lifted pseudo adiabatically with the virtual temperature correction applied (Doswell III and Rasmussen, 1994). The semi-transparent red shaded area denotes the CAPE for a mixed-layer-based parcel. In the hodograph insets, the sfc-1 km, 1–3 km, 3–6 km, and 6–10 km AGL layers are colored in red, green, blue, and olive, respectively. The black arrow extending from the origin of the hodograph denotes the storm motion vector of a left-moving cyclonic supercell based on the Bunkers internal dynamics method (Bunkers et al., 2000). On the lower left corner of each plot, selected relevant convective parameters are presented: MLCAPE, MLCIN, 500–700-hPa lapse rate (MLLR), 0–6-km BWD (BWD6), 0–8-km BWD (BWD8), SRH3, SRH1, SRH0–0.5, magnitude of the Bunkers storm motion for left-moving supercells, and MLLCL heights. (For interpretation of the references to colour in this figure legend, the reader is referred to the web version of this article.)

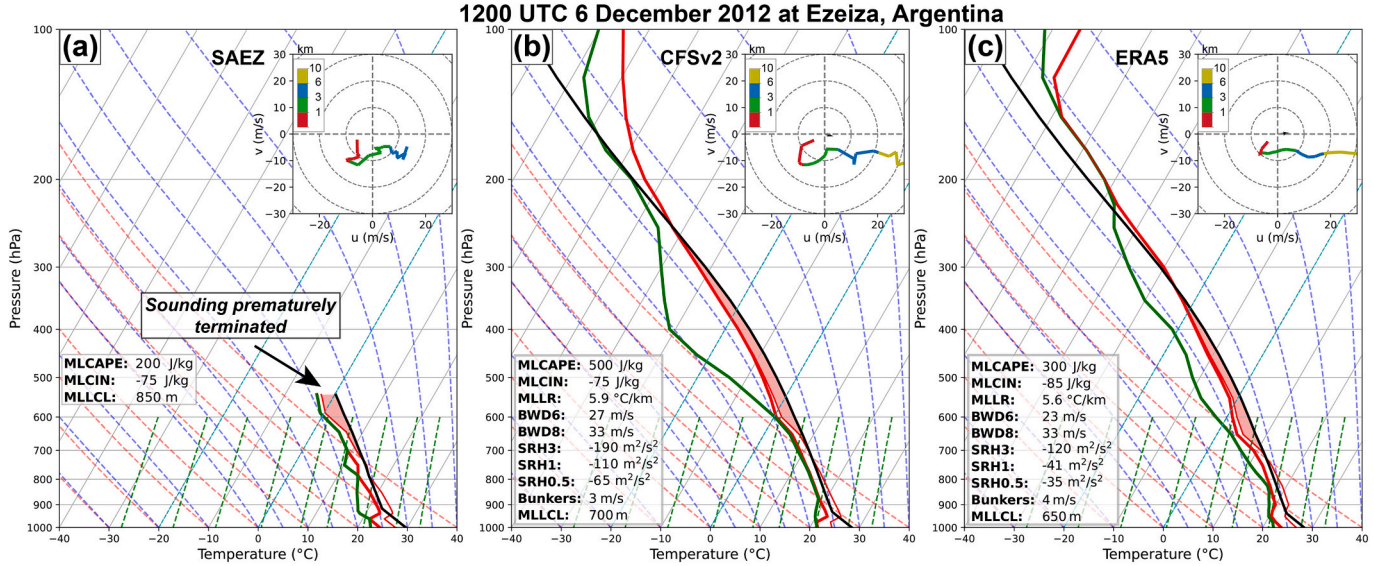

Fig. 13. As in Fig. 11, but valid at 1200 UTC (0900 LST) 6 December 2012.

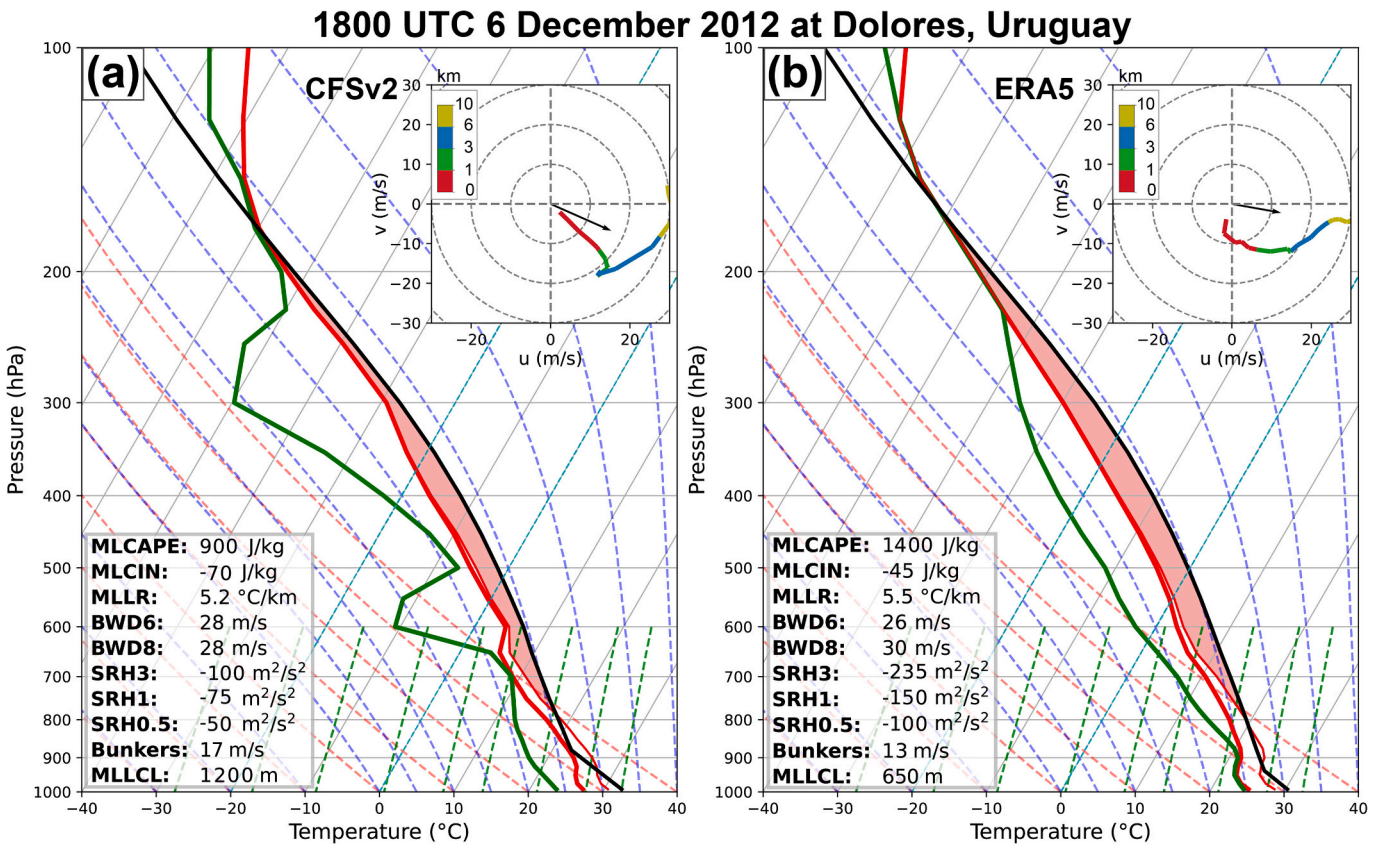

Fig. 14. As in Fig. 12, but valid at 1800 UTC (1500 LST) 6 December 2012.

sector established by warm fronts that traversed toward southern Uruguay. The key feature was the presence of strong LLJs, which promoted vigorous low-level advection of heat and moisture into SWUY and strong low-level shear. On one hand, these results highlight a synoptic-scale setup that is conducive to tornadic supercells in SWUY and likely more generally the entire SESA region and should increase the awareness of forecasters in similar future setups. On the other hand, the general setup that led to the two events is relatively common in SESA severe storm environments and not restricted to tornadic supercells, since it is often associated with severe straight-line winds, large hail, and heavy precipitation events (Lopes and Nascimento, 2024). When this type of setup is in place, the strength of the LLJ is crucial to determine the potential for tornadic storms, especially if it is accompanied by large near-surface SRH (Veloso-Aguila et al., 2023; Lopes and Nascimento, 2024).

Another key goal of this study was to assess the mesoscale environment of the storms and determine whether any relevant features encouraged their formation and tornado production near Dolores. It was shown that both the 2012 and 2016 storms developed in the wake of early-day MCSs (associated with the southward-moving warm fronts and the nose of the LLJ) in air masses that recovered from convective contamination due to abundant solar heating and warm advection. The initiation of the storms occurred near the northern edge of the Parana river delta in eastern Argentina located ~100 km northwest of Dolores. Under the strong northwesterly winds above the boundary layer, the storms moved southeastward toward SWUY and Dolores while maturing into supercells. From this analysis, we conclude that Dolores was impacted by both supercells because of (1) storm formation upstream from SWUY, (2) the high environmental shear that favored storms to mature into tornadic supercells, and (3) storm motion vectors that placed Dolores in the path of the supercells. Regarding point (1), we speculate that storm formation may have been fostered by breeze-type convergence at the northern edge of the Parana river delta, locally augmented by outflow boundaries. This speculation is based mostly on the observation of afternoon formation of enhanced cumulus lines at the northern edge of the Parana river possibly intersected by outflow boundaries inferred from GOES-13 visible imagery during the hours preceding storm formation. The causes for the occurrence of the tornadoes at Dolores is, however, less straightforward. As previously discussed, the synoptic-scale environment was supportive of supercell tornadogenesis in SWUY. With the available observational data, it is impossible to evaluate whether tornadogenesis occurred due to internal supercell dynamics in a tornado-prone environment (Markowski, 2020), interactions with a sheared boundary layer (Markowski, 2024), interactions between mesoscale boundaries (one of which appears to develop based on the terrain near Dolores), or due to a combination of these factors. Based on our results, we can at best point out that forecasters in SWUY concerned with situations similar to the Dolores cases should pay heightened attention to storm initiation and subsequent development into supercells near the northern edge of the Parana river delta when the background environment is conducive to tornadoes. A more profound understanding of the processes that lead to tornadic storms in SWUY and their prediction would benefit from an expansion of the Doppler radar network (and eventual close-range observations) and the use of high-resolution, convection-permitting simulations.

A closer inspection of proximity "pseudo"-soundings from CFSv2 and ERA5 near Dolores reveals that the environment was supportive of strong tornadoes, although this result depended somewhat on which model analysis dataset was considered. For the 2016 tornado—the tornado of higher interest in this study—CFSv2 showed an atmosphere with high conditional instability and vertical wind shear conducive to long-lived tornadic supercells while ERA5 showed a stable environment due to a persistent cold pool from an early MCS. For the 2012 tornado, the environment depicted by CFSv2 is supportive of supercells but loosely favorable to tornadoes because of non-negligible MLCIN and straight low-level hodographs (and modest near-surface SRH). ERA5

depicted an environment that is favorable for tornadic supercells (with higher near-surface SRH) but again showed signs of a spurious cold pool from an early MCS.

Lastly, important questions raised in this study warrant further investigation. The question of more relevance to severe storm forecasting in SWUY concerns the role played by convergence at the northern edge of the Parana river delta in the initiation of storms. Horizontal temperature gradients and attendant breeze circulations at the boundary between land and sea/lakes (King et al., 2003; Sills et al., 2004; Sills and Ashton, 2012; Alexander et al., 2018; Wang et al., 2019) and even between dry land and irrigated crops (Liu et al., 2023; Meng et al., 2024) commonly produce convergence lines that foster deep convection initiation. Such temperature gradients commonly develop along the edges of the Parana river delta as observed by the Landsat-7 ETM+ imager and illustrated in Fig. 15 during the afternoon of a summer, cloudless day. Temperature gradients at the Parana river delta can be large, within 10 to 15°C (10 km)$^{-1}$ in the example provided in Fig. 15. Temperature gradients of these magnitudes and even lesser can easily produce breeze circulations and play a key role in convection initiation and even in tornadogenesis (e.g., Sills et al., 2004). Considering the occurrence of the Dolores tornadoes less than four years apart, it is likely that breeze-induced convergence at the Parana river delta is a crucial, recurrent aspect of storm development and severe weather in SWUY and should be studied in much more detail. Future research to improve the forecasting and nowcasting of severe storms in SWUY should include a thorough statistical analysis of convection initiation in that area using multi-year satellite data products such as the ones used in this study given the scarcity of surface meteorological stations. Results from this type of analysis would provide a better knowledge of the frequency of breeze-induced convection initiation events, the relevance of delta breeze/storm outflow interactions for convection initiation and tornado occurrence, and the synoptic-scale environments that support these mesoscale phenomena. Moreover, a deeper comprehension of the thermodynamic and kinematic features of breeze-induced convection initiation could be achieved through the use of ground-based observational platforms including Doppler lidars, Doppler radars, rawinsondes, and surface meteorological stations (Curry et al., 2017) placed on both sides of the delta edges, but especially on the northern edge where the Dolores storms formed. A simpler and more straightforward approach to study the breezes in the area of interest is to conduct sensitivity numerical simulations to alter the properties of the surface (e.g., moisture content, land and vegetation types) around the Parana river delta and determine its impacts on the initiation of the Dolores storms. Results from such simulations could supplement those from observational studies to aid forecasters antecipte convection initiation on satellite, radar, and convection-permitting numerical data and determine severe weather potential in SWUY a few hours in advance.

Supplementary data to this article can be found online at https://doi.org/10.1016/j.atmosres.2025.107947.

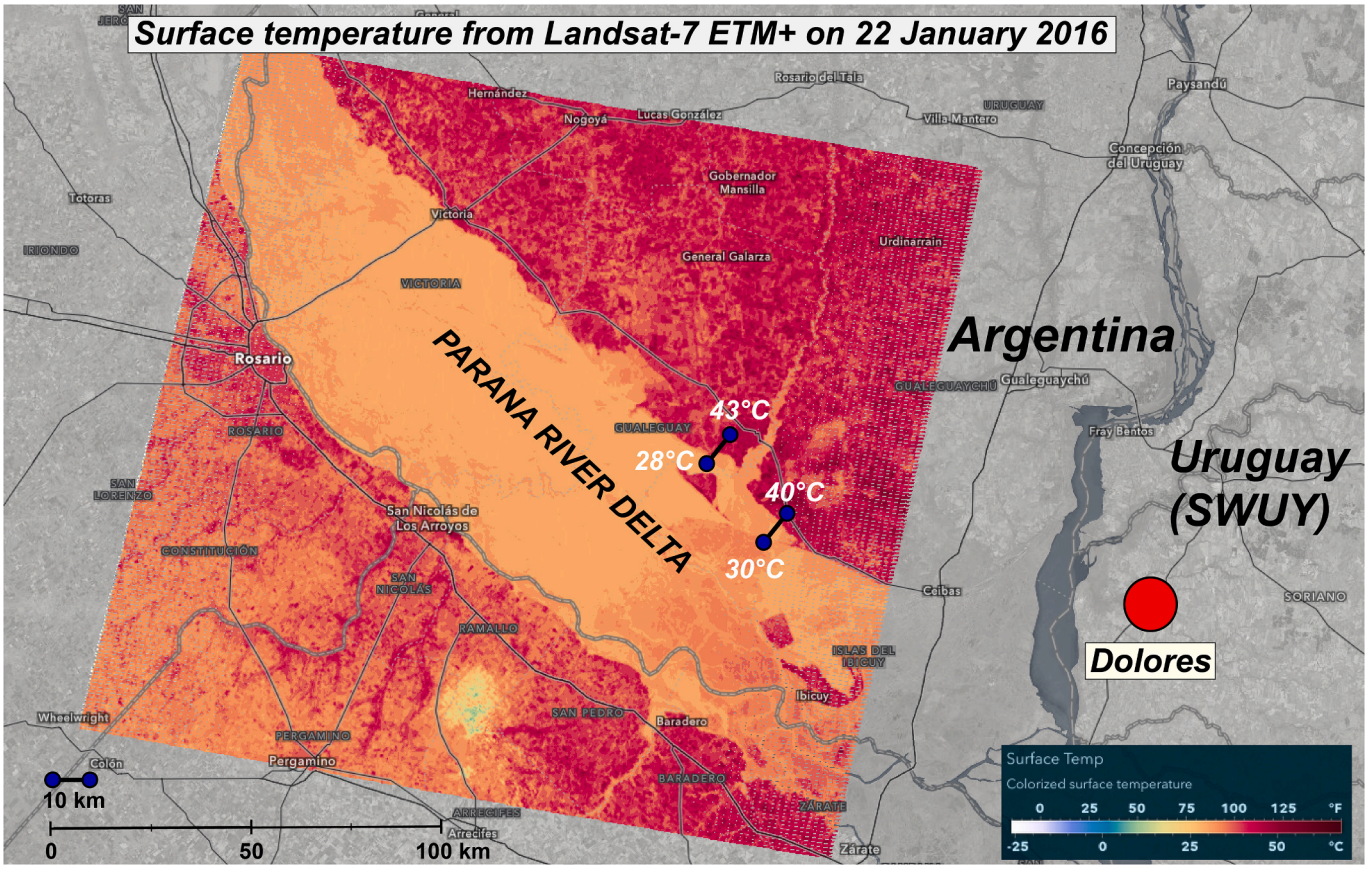

Fig. 15. Surface temperature observed by the Enhanced Thematic Mapper Plus (ETM+) sensor aboard Landsat-7 during the afternoon of 22 January 2016 centered on the Parana river delta near the Argentina-Uruguay border. This cloudless summer day was chosen to easily illustrate the temperature contrast between the delta and the surrounding areas. The strongest horizontal temperature gradient is found between at the northern edge of the delta and around the area where the 2012 and 2016 Dolores supercells initiated. The strength of the horizontal temperature gradient is illustrated at two nearby areas of the northern delta region, indicated by two pairs of blue circles along with Landsat-estimated temperatures (annotated in white). In each pair, the northernmost (southernmost) circle is located on the warm (cool) side of the northern edge of the delta and the circles are located 10 km apart. The red circle denotes the location of Dolores. (For interpretation of the references to colour in this figure legend, the reader is referred to the web version of this article.)

CRediT authorship contribution statement

Maurício I. Oliveira: Writing – review & editing, Writing – original draft, Visualization, Validation, Supervision, Software, Resources, Project administration, Methodology, Investigation, Formal analysis, Data curation, Conceptualization. **Murilo M. Lopes:** Writing – review & editing, Visualization, Validation, Software, Project administration, Methodology, Investigation, Formal analysis, Data curation, Conceptualization. **Vitor Goede:** Writing – review & editing, Visualization, Software, Methodology, Investigation, Formal analysis, Data curation. **Marcelo Barreiro:** Writing – review & editing, Visualization, Validation, Resources, Methodology, Investigation, Formal analysis, Data curation. **Paola M. Salio:** Writing – review & editing, Validation, Resources, Project administration, Methodology, Investigation, Formal analysis, Data curation. **Eliton L. Figueiredo:** Writing – review & editing, Visualization, Software, Investigation, Formal analysis. **Ming Xue:** Writing – review & editing, Investigation, Formal analysis.

Declaration of competing interest

The authors declare that they have no known competing financial interests or personal relationships that could have appeared to influence the work reported in this paper.

Data availability

Data will be made available on request.

Acknowledgements

The authors appreciate the insightful comments and suggestions from Dr. David Sills and two anonymous reviewers for their comprehensive comments, which contributed to an improved version of this article. The authors are grateful to Mr. Arlington Perez and Mr. Edward Peña for generously granting permission to use their videos in our Figs. 2–6. We thank Drs. Jim LaDue and Mike Coniglio for the helpful insights that helped improve the damage analysis of the 15 April 2016 tornado. The first author also thanks Dr. Matilde Ungerovich for early and helpful discussions on the 2016 tornado case. Several figures were generated using open-sourced Python packages including Matplotlib (Hunter, 2007), Pandas (McKinney et al., 2011), Numpy (Harris et al., 2020), Xarray (Hoyer and Hamman, 2017), and Metpy (May et al., 2022).

References

Adlerman, E.J., Droegemeier, K.K., Davies-Jones, R., 1999. A numerical simulation of cyclic mesocyclogenesis. J. Atmos. Sci. 56, 2045–2069.
Agee, E., Snow, J., Clare, P., 1976. Multiple vortex features in the tornado cyclone and the occurrence of tornado families. Mon. Weather Rev. 104, 552–563.
Agostinho, A.M., Antonio, C.A., Figueiredo, J.C., 2005. Tornados do Outono de 2004 no Interior Paulista. In: XII Symp. on Remote Sensing. INPE, pp. 2819–2826.
Alexander, L.S., Sills, D.M., Taylor, P.A., 2018. Initiation of convective storms at low-level mesoscale boundaries in southwestern Ontario. Weather Forecast. 33, 583–598.
Atkins, N.T., Buttler, K.M., Flynn, K.L., Wakimoto, R.M., 2014. An integrated damage, visual, and radar analysis of the 2013 Moore, Oklahoma, EF5 tornado. Bull. Am. Meteorol. Soc. 95, 1549–1561.
Bai, L., Meng, Z., Huang, L., Yan, L., Li, Z., Mai, X., Huang, Y., Yao, D., Wang, X., 2017. An integrated damage, visual, and radar analysis of the 2015 Foshan, Guangdong, EF3 tornado in China produced by the landfalling typhoon Mujigae (2015). Bull. Am. Meteorol. Soc. 98, 2619–2640.
Barreiro, M., Cazes-Boezio, G., Saucedo, M., Silva, A., 2016. Tornado Registrado en la Ciudad de Dolores en 15/04/2016. Technical Report. Instituto Uruguayo de Meteorología.
Barrett, B.S., Marin, J.C., Jacques-Coper, M., 2020. A multiscale analysis of the tornadoes of 30–31 May 2019 in south-central Chile. Atmos. Res. 236, 104811.
Becker, V. 2016. Tornado en Uruguay Deja Cuatro Muertos y 200 Heridos, CNN URL https://cnnespanol.cnn.com/2016/04/15/tornado-en-uruguay-deja-cuatro-muertos-y-siete-heridos-graves/.
Beer, M., 2023. Traumas, Deudas y Muerte a Siete Años del Tornado de Dolores El País URL https://www.elpais.com.uy/informacion/sociedad/traumas-deudas-y-muerte-a-siete-anos-del-tornado-de-dolores.
Bluestein, H.B., Snyder, J.C., Houser, J.B., 2015. A multiscale everview of the El Reno, Oklahoma, tornadic supercell of 31 May 2013. Weather Forecast. 30, 525–552.
Bluestein, H.B., Lindsey, D.T., Bikos, D., Reif, D.W., Wienhoff, Z.B., 2019. The relationship between overshooting tops in a tornadic supercell and its radar-observed evolution. Mon. Weather Rev. 147, 4151–4176.
Borque, P., Vidal, L., Rugna, M., Lang, T.J., Nicora, M.G., Nesbitt, S.W., 2020. Distinctive signals in 1-min observations of overshooting tops and lightning activity in a severe supercell thunderstorm. J. Geophys. Res. Atmos. 125 e2020JD032856.
Brooks, H.E., Lee, J.W., Craven, J.P., 2003. The spatial distribution of severe thunderstorm and tornado environments from global reanalysis data. Atmos. Res. 67, 73–94.
Brooks, H.E., Doswell III, C.A., Zhang, X., Chernokulsky, A.A., Tochimoto, E., Hanstrum, B., de Lima Nascimento, E., Sills, D.M., Antonescu, B., Barrett, B., 2019. A century of progress in severe convective storm research and forecasting. Meteorol. Monogr. 59, 18–21.
Bunkers, M.J., Klimowski, B.A., Zeitler, J.W., Thompson, R.L., Weisman, M.L., 2000. Predicting supercell motion using a new hodograph technique. Weather Forecast. 15, 61–79.
Bunkers, M.J., Johnson, J.S., Czepyha, L.J., Grzywacz, J.M., Klimowski, B.A., Hjelmfelt, M.R., 2006. An observational examination of long-lived supercells. Part II: environmental conditions and forecasting. Weather Forecast. 21, 689–714.
Chen, J., Zhu, X., Vogelmann, J.E., Gao, F., Jin, S., 2011. A simple and effective method for filling gaps in Landsat ETM+ SLC-Off images. Remote Sens. Environ. 115, 1053–1064.
Coffer, B.E., Parker, M.D., Thompson, R.L., Smith, B.T., Jewell, R.E., 2019. Using near-ground storm relative helicity in supercell tornado forecasting. Weather Forecast. 34, 1417–1435.
Curry, M., Hanesiak, J., Kehler, S., Sills, D.M., Taylor, N.M., 2017. Ground-based observations of the thermodynamic and kinematic properties of Lake-Breeze Fronts in southern Manitoba, Canada. Bound.-Lay. Meteorol. 163, 143–159.
dos Santos, L.O., Nascimento, E.L., Allen, J.T., 2023. Discriminant analysis for severe storm environments in south-central Brazil. Mon. Weather Rev. 151, 2659–2681.
Doswell III, C.A., Rasmussen, E.N., 1994. The effect of neglecting the virtual temperature correction on CAPE calculations. Weather Forecast. 9, 625–629.
Dowell, D.C., Bluestein, H.B., 2002. The 8 June 1995 Mclean, Texas, storm. Part II: Cyclic tornado formation, maintenance, and dissipation. Mon. Weather Rev. 130, 2649–2670.
Durañona, V., 2015. Extreme Wind Climate of Uruguay. Reportes Técnicos, p. 263.
Dyer, R.C., 1988. Remote sensing identification of tornado tracks in Argentina, Brazil, and Paraguay. Photogram. Eng. Remote Sens. 54, 1429–1435.
Ferreira, V., Goede, V., de Lima Nascimento, E., 2022. An environmental and polarimetric study of the 19 November 2015 supercell and multiple-vortex tornado in Marechal Cândido Rondon, Southern Brazil. Meteorol. Atmos. Phys. 134, 82.
Fujita, T.T., 1971. Proposed characterization of tornadoes and hurricanes by area and intensity. In: SMRP Research Paper. University of Chicago, Satellite and Mesometeorology Research Project, 42 p.
Fujita, T.T., 1973. Tornadoes around the world. Weatherwise 26, 56–83.
Fujita, T.T., 1981. Tornadoes and downbursts in the context of generalized planetary scales. J. Atmos. Sci. 38, 1511–1534.
Fujita, T.T., 1993. Plainfield tornado of August 28, 1990. In: Washington DC American Geophysical Union Geophysical Monograph Series, 79, pp. 1–17.
Garner, J.M., Iwasko, W.C., Jewel, T.D., Thompson, R.L., Smith, B.T., 2021. An environmental study on tornado pathlength, longevity, and width. Weather Forecast. 36, 1471–1490.
Harris, C.R., Millman, K.J., Van Der Walt, S.J., Gommers, R., Virtanen, P., Cournapeau, D., Wieser, E., Taylor, J., Berg, S., Smith, N.J., et al., 2020. Array programming with numpy. Nature 585, 357–362.
Hersbach, H., Bell, B., Berrisford, P., Hirahara, S., Horányi, A., Muñoz-Sabater, J., Nicolas, J., Peubey, C., Radu, R., Schepers, D., et al., 2020. The ERA5 global reanalysis. Q. J. Roy. Meteorol. Soc. 146, 1999–2049.
Houser, J.L., Bluestein, H.B., Snyder, J.C., 2016. A finescale radar examination of the tornadic debris signature and weak-echo reflectivity band associated with a large, violent Tornado. Mon. Weather Rev. 144, 4101–4130. https://doi.org/10.1175/MWR-D-15-0408.1.
Hoyer, S., Hamman, J., 2017. Xarray: N-D labeled arrays and datasets in Python. J. Open Res. Softw. 5, 10.
Huang, W., Xue, M., 2023. Subvortices within a numerically simulated tornado: the role of unstable vortex rossby waves. J. Atmos. Sci. 80, 2503–2529.
Hunter, J.D., 2007. Matplotlib: a 2D graphics environment. Comput. Sci. Eng. 9, 90–95.
King, P.W., Leduc, M.J., Sills, D.M., Donaldson, N.R., Hudak, D.R., Joe, P., Murphy, B.P., 2003. Lake breezes in southern Ontario and their relation to tornado climatology. Weather Forecast. 18, 795–807.
Klemp, J.B., 1987. Dynamics of tornadic thunderstorms. Annu. Rev. Fluid Mech. 19, 369–402.
Knupp, K.R., Murphy, T.A., Coleman, T.A., Wade, R.A., Mullins, S.A., Schultz, C.J., Schultz, E.V., Carey, L., Sherrer, A., McCaul Jr., E.W., et al., 2014. Meteorological overview of the devastating 27 April 2011 tornado outbreak. Bull. Am. Meteorol. Soc. 95, 1041–1062. https://doi.org/10.1175/BAMS-D-11-00229.1.
Liu, H., Meng, Z., Zhu, Y., Huang, Y., 2023. Convection initiation associated with a boundary layer convergence line over a real-world sharp vegetation-contrast area. Mon. Weather Rev. 151, 1189–1212.
Lopes, M.M., dos Santos, L.O., 2022. Climatology of Tornadoes in South America Tornado Alley. In: 30th Conference on Severe Local Storms, AMS.

Lopes, M.M., Nascimento, E.L., 2020. Use of remote sensing via satellite in the identification of tornado damage paths in a severe weather event in Rio Grande do Sul. Ciênc. Nat. 42, e8.
Lopes, M.M., Nascimento, E.L., 2024. Atmospheric environments associated with tornadoes in southern Brazil and neighboring areas as compared to other modes of convective hazards. Climate Dynam. 1–27.
Marengo, J.A., Soares, W.R., Saulo, C., Nicolini, M., 2004. Climatology of the low-level jet east of the Andes as derived from the NCEP–NCAR reanalyses: characteristics and temporal variability. J. Climate 17, 2261–2280.
Marín, J.C., Barrett, B.S., Pozo, D., 2021. The tornadoes of 30–31 May 2019 in south-central Chile: sensitivity to topography and SST. Atmos. Res. 249, 105301.
Markowski, P.M., 2020. What is the intrinsic predictability of tornadic supercell thunderstorms? Mon. Weather Rev. 148, 3157–3180.
Markowski, P.M., 2024. A new pathway for tornadogenesis exposed by numerical simulations of supercells in turbulent environments. J. Atmos. Sci. 81, 481–518.
May, R.M., Goebbert, K.H., Thielen, J.E., Leeman, J.R., Camron, M.D., Bruick, Z., Bruning, E.C., Manser, R.P., Arms, S.C., Marsh, P.T., 2022. Metpy: a meteorological Python library for data analysis and visualization. Bull. Am. Meteorol. Soc. 103, E2273–E2284.
McDonald, J.R., Mehta, K.C., 2006. A recommendation for an Enhanced Fujita Scale (EF-Scale). Wind Science and Engineering Center, Texas Tech University.
McKinney, W., et al., 2011. Pandas: a foundational Python library for data analysis and statistics. In: Python for High Performance and Scientific Computing, 14, pp. 1–9.
Meng, Z., Meng, X., Wang, C., Huang, Y., Zhang, S., Liu, H., Zhang, M., Liu, Y., Huang, H., Su, L., et al., 2024. Desert–oasis convergence line and deep convection experiment (DECODE). Bull. Am. Meteorol. Soc. 105, E2355–E2384.
Montini, T.L., Jones, C., Carvalho, L.M., 2019. The South American low-level jet: a new climatology, variability, and changes. J. Geophys. Res. Atmos. 124, 1200–1218.
Nascimento, E.L., Doswell III, C., 2006. The need for an improved documentation of severe thunderstorms and tornadoes in South America. In: Symp. on the Challenges of Severe Convective Storms.
Nascimento, E.L., Held, G., Gomes, A.M., 2014. A multiple-vortex tornado in southeastern Brazil. Mon. Weather Rev. 142, 3017–3037. https://doi.org/10.1175/MWR-D-13–00319.1.
Nascimento, E.L., Foss, M., Ferreira, V., Brooks, H.E., 2016. An updated and expanded climatology of severe weather parameters for subtropical South America as derived from upper air observations and CFSR-CFSv2 data. In: Proceedings of 28th Conference on Severe Local Storms, American Meoteological Society, Portland. URL. https://ams.confex.com/ams/28SLS/webprogram/Paper300887.html.
Oliveira, M.I., Nascimento, E.L., Kannenberg, C., 2018. A new look at the identification of low-level jets in South America. Mon. Weather Rev. 146, 2315–2334.
Oliveira, M.I., Xue, M., Roberts, B.J., Wicker, L.J., Yussouf, N., 2019. Horizontal vortex tubes near a simulated tornado: three-dimensional structure and kinematics. Atmosphere 10, 716. https://doi.org/10.3390/atmosl0110716.
Oliveira, M.I., Puhales, F.S., Nascimento, E.L., Anabor, V., 2022a. Integrated damage, visual, remote sensing, and environmental analysis of a strong tornado in southern Brazil. Atmos. Res. 274, 106188.
Oliveira, M.I., Xue, M., Roberts, B., 2022b. Trailing horizontal vortices in observed and numerically simulated tornadoes. Bull. Am. Meteorol. Soc. 103, E2768–E2790.
Piscitelli, F.M., Ruiz, J.J., Negri, P., Salio, P., 2022. A multiyear radar-based climatology of supercell thunderstorms in central-eastern Argentina. Atmos. Res. 277, 106283.
Pita, G.L., de Schwarzkopf, M.L.A.d., 2016. Urban downburst vulnerability and damage assessment from a case study in Argentina. Nat. Hazards 83, 445–463.
Rasmussen, E.N., 2003. Refined supercell and tornado forecast parameters. Weather Forecast. 18, 530–535. https://doi.org/10.1175/1520–0434(2003)18<530:RSATFP>2.0.CO;2.
Rasmussen, E.N., Blanchard, D.O., 1998. A baseline climatology of sounding-derived supercell and tornado forecast parameters. Weather Forecast. 13, 1148–1164.
Rasmussen, K.L., Zuluaga, M.D., Houze, R.A., 2014. Severe convection and lightning in subtropical South America. Geophys. Res. Lett. 41, 7359–7366.
Ribeiro, B.Z., Seluchi, M.E., Chou, S.C., 2016. Synoptic climatology of warm fronts in southeastern South America. Int. J. Climatol. 36, 644–655.
Rose, S.F., Hobbs, P.V., Locatelli, J.D., Stoelinga, M.T., 2004. A 10-yr climatology relating the locations of reported tornadoes to the quadrants of upper-level jet streaks. Weather Forecast. 19, 301–309.
Saha, S., Moorthi, S., Pan, H.L., Wu, X., Wang, J., Nadiga, S., Tripp, P., Kistler, R., Woollen, J., Behringer, D., et al., 2010. The NCEP climate forecast system reanalysis. Bull. Am. Meteorol. Soc. 91, 1015–1057.
Saha, S., Moorthi, S., Wu, X., Wang, J., Nadiga, S., Tripp, P., Behringer, D., Hou, Y.T., Chuang, H.y., Iredell, M., Ek, M., Meng, J., Yang, R., Mendez, M.P.n., Dool, H.v.d., Zhang, Q., Wang, W., Chen, M., Becker, E., 2014. The NCEP climate forecast system version 2. J. Climate 27, 2185–2208.
Salio, P., Bechis, H., Ribeiro, B.Z., de Lima Nascimento, E., Galligani, V., Garcia, F., Alvarenga, L., Imaz, M.d.l.M.A., Baissac, D.M., Barle, M.F., et al., 2024. Towards a South American high impact weather reports database. Bull. Am. Meteorol. 105, E1204–E1217.
Salio, P., Nicolini, M., Saulo, A.C., 2002. Chaco low-level jet events characterization during the austral summer season. J. Geophys. Res. Atmos. 107. ACL–32.
Salio, P., Nicolini, M., Zipser, E.J., 2007. Mesoscale convective systems over southeastern South America and their relationship with the South American low-level jet. Mon. Weather Rev. 135, 1290–1309.
Sasaki, C.R., Rowe, A.K., McMurdie, L.A., Rasmussen, K.L., 2022. New insights into the South American low-level jet from RELAMPAGO observations. Mon. Weather Rev. 150, 1247–1271.
Saulo, C., Ruiz, J., Skabar, Y.G., 2007. Synergism between the low-level jet and organized convection at its exit region. Mon. Weather Rev. 135, 1310–1326.
Schwarzkopf, M.L.A.d., 1988. Climatologia de los Efectos de la Conveccion Severa en la Republica Argentina. Ph.D. thesis.. Universidad de Buenos Aires. Facultad de Ciencias Exactas y Naturales.
Schwarzkopf, M.L.A.d., Rosso, L., 1982. Severe storms and tornadoes in Argentina. In: Preprints, 12th Conf. on Severe Local Storms, San Antonio, TX. Amer. Meteor. Soc, p. 62.
Seluchi, M.E., Saulo, A.C., Nicolini, M., Satyamurty, P., 2003. The northwestern Argentinean low: a study of two typical events. Mon. Weather Rev. 131, 2361–2378.
Sills, D.M., Ashton, A., 2012. Examination of a remarkable great lake-spawned tornadic supercell: the 2011 Goderich Ontario F3 tornado event. In: Preprints, 26th Conf. on Severe Local Storms, Nashville, TN. Amer. Meteor. Soc.
Sills, D.M., Wilson, J.W., Joe, P.I., Burgess, D.W., Webb, R.M., Fox, N.I., 2004. The 3 November tornadic event during Sydney 2000: storm evolution and the role of low-level boundaries. Weather Forecast. 19, 22–42.
Silva Dias, M.A.F., 2011. An increase in the number of tornado reports in Brazil. Weather Clim. Soc. 3, 209–217. https://doi.org/10.1175/2011WCAS1095.1.
Silva Dias, M.A.F., Grammelsbacher, E.A., 1991. A Possível Ocorrência de Tornado em São Paulo no Dia 26 de Abril de 1991: Um Estudo de Caso. Revista Brasileira de Meteorologia 6, 513–522.
Taszarek, M., Allen, J.T., Marchio, M., Brooks, H.E., 2021. Global climatology and trends in convective environments from ERA5 and rawinsonde data. NPJ Clim. Atmos. Sci. 4, 35.
Thompson, R.L., Edwards, R., 2000. An overview of environmental conditions and forecast implications of the 3 May 1999 Tornado outbreak. Weather Forecast. 15, 682–699.
Thompson, R.L., Edwards, R., Hart, J.A., Elmore, K.L., Markowski, P., 2003. Close proximity soundings within supercell environments obtained from the rapid update cycle. Weather Forecast. 18, 1243–1261. https://doi.org/10.1175/1520–0434(2003)018<1243:CPSWSE>2.0.CO;2.
Thompson, R.L., Mead, C.M., Edwards, R., 2007. Effective storm-relative helicity and bulk shear in supercell thunderstorm environments. Weather Forecast. 22, 102–115.
Thompson, R.L., Smith, B.T., Grams, J.S., Dean, A.R., Broyles, C., 2012. Convective modes for significant severe thunderstorms in the contiguous United States. Part II: supercell and QLCS tornado environments. Weather Forecast. 27, 1136–1154.
Uccellini, L.W., Johnson, D.R., 1979. The coupling of upper and lower tropospheric jet streaks and implications for the development of severe convective storms. Mon. Weather Rev. 107, 682–703.
Ungerovich, M., Barreiro, M., 2019. Dynamics of extreme rainfall events in summer in southern Uruguay. Int. J. Climatol. 39, 3655–3667.
Ungerovich, M., Barreiro, M., Kalemkerian, J., 2023. Simulation of extreme rainfall events in Uruguay: role of initialization and large scale dynamics. Atmos. Res. 106842.
Veloso-Aguila, D., Rasmussen, K.L., Maloney, E.D., 2023. Tornadoes in Southeast South America: Mesoscale to Planetary-Scale Environments. Month. Weather. Rev. 152, 295–318.
Vicencio, J., Rondanelli, R., Campos, D., Valenzuela, R., Garreaud, R., Reyes, A., Padilla, R., Abarca, R., Barahona, C., Delgado, R., et al., 2021. The Chilean tornado outbreak of May 2019: synoptic, mesoscale, and historical contexts. Bull. Am. Meteorol. Soc. 102, E611–E634.
Wakimoto, R.M., Wienhoff, Z., Reif, D., Bluestein, H.B., Lewellen, D.C., 2022. The Dodge City tornadoes on 24 May 2016: understanding cycloidal marks in surface damage tracks and further analysis of the debris cloud. Mon. Weather Rev. 150, 1233–1246.
Wang, C.C., Kirshbaum, D.J., Sills, D.M., 2019. Convection initiation aided by Lake-Breeze convergence over the Niagara Peninsula. Mon. Weather Rev. 147, 3955–3979.
Wurman, J., Kosiba, K., 2013. Finescale radar observations of tornado and mesocyclone structures. Weather Forecast. 28, 1157–1174.
Wurman, J., Kosiba, K., Robinson, P., Marshall, T., 2014. The role of multiple-vortex tornado structure in causing storm researcher fatalities. Bull. Am. Meteorol. Soc. 95, 31–45.